WAVELET ESTIMATION AND DEBUBBLING USING MINIMUM ENTROPY DECONVOLUTION AND TIME DOMAIN LINEAR INVERSE METHODS.

by

SHLOMO LEVY

B.Sc., University of California Los Angeles, 1977

A THESIS SUBMITTED IN PARTIAL FULFILLMENT OF THE REQUIREMENTS FOR THE DEGREE OF MASTER OF SCIENCE

in

THE FACULTY OF GRADUATE STUDIES

(Department of Geophysics and Astronomy)

We accept this thesis as conforming to the required standard:

THE UNIVERSITY OF BRITISH COLUMBIA.

June, 1979

In presenting this thesis in partial fulfilment of the requirements for an advanced degree at the University of British Columbia, I agree that the Library shall make it freely available for reference and study. I further agree that permission for extensive copying of this thesis for scholarly purposes may be granted by the Head of my Department or by his representatives. It is understood that copying or publication of this thesis for financial gain shall not be allowed without my written permission.

Department of GEOPHYSICS AND ASTRONOMY

The University of British Columbia
2075 Wesbrook Place
Vancouver, Canada
V6T 1W5

Date AUG - 15 - 1979

ABSTRACT

A new and different approach to the solution of the normal equations of minimum entropy deconvolution (MED) is developed. This approach which uses singular value decomposition in the iterative solution of the MED equations increases the signal-to-noise ratio of the deconvolved output and enhances the resolution of MED.

The problem of deconvolution, and in particular wavelet estimation, is formulated as a linear inverse problem. Both generalized linear inverse methods and Backus-Gilbert inversion are considered. The proposed wavelet estimation algorithm uses the MED output as a first approximation to the earth response. The approximated response and the observed seismograms serve as an input to the inversion schemes and the outputs are the estimated wavelets. The remarkable performance of the linear inverse schemes for cases of highly noisy data is demonstrated.

A debubbling example is used to show the completeness of the linear inverse schemes. First the wavelet estimation part was carried out and then the debubbling problem was formulated as a generalized linear inverse problem which was solved using the estimated wavelet.

This work demonstrates the power of the linear inverse schemes when dealing with highly noisy data.

TABLE OF CONTENTS

LIST OF TABLES

LIST OF FIGURES

ACKNOWLEDGEMENTS

I would like to express my gratitude to my supervisor Dr. R.M. Clowes for his encouragement, help and constructive remarks during every stage of the work.

For his most stimulating course on linear inverse methods which triggered the larger part of this work as well as for his most helpful suggestions and remarks I wish to express my thanks to Dr. D.W. Oldenburg.

My deepest thanks to Dr. T.J. Ulrych for his stimulating discussions and suggestions which led to a large part of this work.

Special thanks go to my friend Mr. C.J. Walker for his help and suggestions.

Synthetic seismograms were generated by computer program STPSYN written by R.A. Wiggins and D.V. Helmberger.

Funding for this project was provided through operating grant A7707 of the Natural Sciences and Engineering Research Council Canada and research grant from the University of British Columbia. Additional funds were donated by Mobil Oil Canada Ltd., Shell Canada Resources Ltd. and Chevron Standard Ltd.

CHAPTER 1

Introductory Remarks

Seismic methods are commonly used to aid the study of the earth's interior. Employing the assumption of a layered earth, one uses the fact that on passing from one layer to another the energy of an elastic wave is separated into a transmitted and reflected component. The amount of energy reflected or refracted is basically a function of the angle of incidence of the wave at the interface and the acoustic impedance (density times velocity) of both layers. A geophone placed on the earth's surface responds to this reflected and refracted energy and its output, after amplification, is recorded (the seismogram). The task of the seismologist is to interpret the seismogram. That is, the seismologist is looking for the geological model of the subsurface which can be inferred from the seismogram.

To make things clearer, consider the following example; Assume a three layer model as shown in Figure 1. For simplicity let these be liquid layers (no shear waves), with density and velocity as shown in Figure 1, and the condition $\rho_1 V_1 < \rho_2 V_2 > \rho_3 V_3$. Neglect the direct wave and assume that only reflected energy corresponding to the rays 1 and 2 in Figure 1 has been recorded on the seismogram.

Define two time series: 1) the source wavelet, which represents the shape of the signal before it was transferred

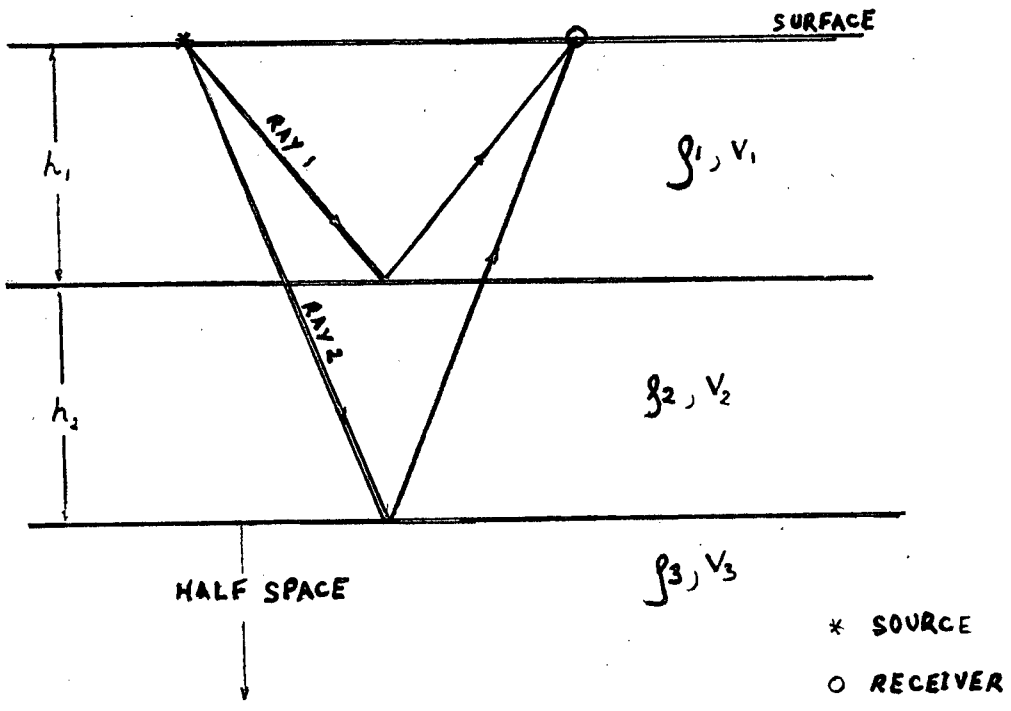

Figure 1

Three liquid layer model

through the ground; 2) the impulse response series. The latter is a time series which consists of zeros everywhere except for the times which correspond exactly to the arrival times of reflected or refracted energy. For these particular times, the impulse response becomes a spike with an amplitude which reflects the energy left in the signal after travelling the path specified by the particular ray.

Assume that the source wavelet is a Ricker wavelet, and using the model of Figure 1, the corresponding impulse response can be derived. Figure 2 shows this time series together with

the seismogram which is the convolution of the impulse response and the source wavelet. If we assume vertical incidence

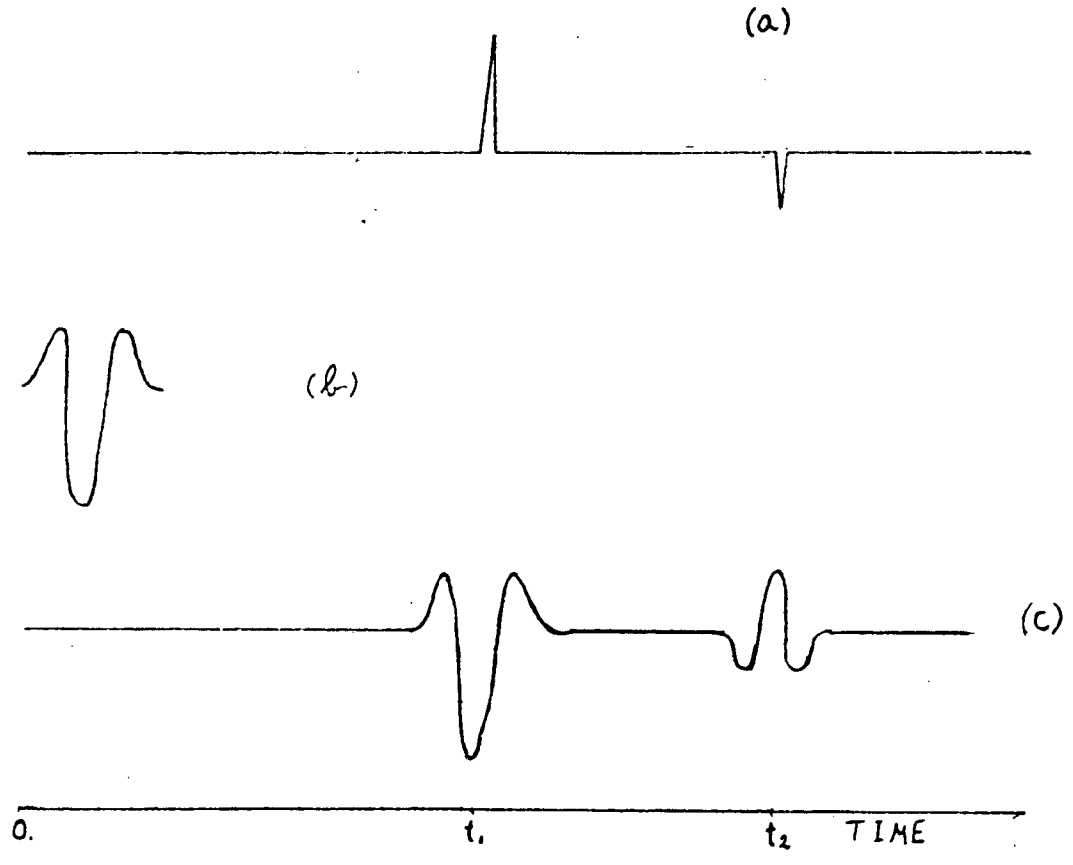

Figure 2

(a) Impulse response for the model of Figure 1. (b) Ricker wavelet as source waveform. (c) The seismogram (convolution of (a) and (b)).

reflection in this example, then the two-way reflection traveltimes to the two layers are $t_1 = 2 \cdot h_1 / V_1$ and $t_2 = 2h_1 / V_1 + 2h_2 / V_2$.

The example shows that the impulse response series reflects the subsurface geology and hence it is the immediate target of the seismologist. If a seismogram is assumed to be the

convolution of a source wavelet with the earth's response, then identifying and deriving the impulse response function is termed "deconvolution".

This work is devoted to the deconvolution problem in general and, in particular, to the debubbling problem. This is a special case of the general deconvolution problem which arises under particular physical conditions. To solve these problems, minimum entropy deconvolution and linear inversion techniques are developed.

CHAPTER 2

Minimum Entropy Deconvolution Using Matrix Spectral Decomposition.

INTRODUCTION

The concept of minimum entropy deconvclution which was introduced by Wiggins (1977) presents a useful tool to aid seismic interpretation. This deconvolution technique searches for a filter F which, when convolved with an input signal X, will convert that signal to an output Y which has a "simple" appearance.

$$(1) \qquad Y=X*F$$

where * denotes convolution.

Wiggins (1977) defined "'simple' to mean that each desired signal consist of a few large spikes of unknown sign or location separated by nearly zero terms". Although it is a good method, MED processing tends to enhance large amplitude impulses compared to smaller amplitude ones and thereby causes some loss of valuable information. A modification of MED has been proposed by Ooe and Ulrych (1979) who introduced the exponential transformation with a modified simplicity norm. They have shown that their approach provides a balance between the noise suppression effect of MED and the ability to recover small

amplitude impulses.

In this work we take the original version of MED (Wiggins 1977) and improve its performance by using a different method of solving the normal equations. In particular we assume that the noisy components of the solution are mainly associated with the small eigenvalues of the autocorrelation matrix. We write the solution as a weighted summation of the eigenvectors of the autocorrelation matrix and reject those components of the solution which are associated with the smaller eigenvalues.

THEORY

Following the approach of Wiggins (1977), we write equation (1) in its time series representation :

$$(2) \qquad Y_{i,j} = \sum_{k=1}^{Nf} F_k \cdot X_{i,j-k+1}$$

where i is the trace index (i=1,...,Ns),

j is the time index (j=1,...., Nt),

Nf is the length of the filter,

Ns is the number of trace segments,

and Nt is the number of time samples in a trace.

The varimax norm V given in equation (3) below is a norm which measures the simplicity of a signal. The larger V is the more "simple" is the signal. For a detailed discussion on simplicity norms the reader is referred to Harman(1960).

$$(3) \quad V = \sum_{i=1}^{N_s} \sum_{j=1}^{N_t} y_{i,j}^4 \Big/ \left(\sum_{j=1}^{N_t} y_{i,j}^2 \right)^2$$

Since we are looking for the filter which will maximize the varimax (simplest possible appearance of the output trace); we proceed by taking the gradient of V, setting it equal to zero and solving :

$$\frac{\partial V}{\partial F_k} = 0 = \sum_i \frac{\partial V_i}{\partial F_k} =$$

$$(4) \quad \sum_i \left\{ 4 V_i U_i^{-1} \sum_j y_{i,j} \frac{\partial y_{i,j}}{\partial F_k} - 4 U_i^{-2} \sum_j y_{i,j}^3 \frac{\partial y_{i,j}}{\partial F_k} \right.$$

$$(4a) \quad U_i = \sum_j y_{i,j}^2$$

from equation (2) we have:

$$(5) \quad \frac{\partial y_{i,j}}{\partial F_k} = x_{i,j-k+1}$$

substituting equation (5) into (4) we get:

$$(6)\quad \sum_{\ell} F_{\ell} \sum_{i} V_i U_i^{-1} \sum_{j} X_{i,j-\ell+1} X_{i,j-k+1} = \sum_{i} U_i^{-2} \sum_{j} Y_{i,j}^{s} X_{i,j-k+1}$$

which can be written in a matrix form as

$$(7)\quad A \cdot \bar{F} = \bar{G}$$

where

A is a weighted autocorrelation matrix,

G is a weighted crosscorrelation vector,

and F is the vector of desired filter coefficients.

Equation (7) is highly nonlinear but it can be solved by an iterative scheme. An initial filter F^0 is proposed and convolved with the input series to give Y^0. Through equations (3), (4a) and (6), the latter enables calculation of the weighted crosscorrelation G^0, and the weighted autocorrelation matrix A^0. Having G^0 and A^0, we can solve for an updated filter F^1. Then the procedure can be repeated until the varimax norm changes very little with subsequent iterations. Wiggins (1977) used the Levinson recursion algorithm for the solution of (7) in order to implement this iterative procedure.

In this paper, we take a different approach. The set of equations (7) is solved by decomposition of matrix A into its spectral components (Lanczos 1961), and finding its inverse. For this procedure A is decomposed as shown below :

$$(8)\quad A = R \Lambda R^{T}$$

where R is a matrix whose columns consist of the eigenvectors of matrix A.

Λ is the diagonal matrix consisting of the eigenvalues of A in decreasing order. $\Lambda = \text{diag}\{\lambda_1, \lambda_2 \ldots \lambda_N\}$ with $\lambda_1 > \lambda_2 > \ldots$

and R^T is the transpose of R.

A is a symmetric, positive definite, Toeplitz matrix. The inverse of A is given by :

$$A^{-1} = R \Lambda^{-1} R^T \tag{9}$$

Substituting equation (9) into (7) we obtain :

$$\bar{F} = R \Lambda^{-1} R^T \bar{G} \tag{10}$$

writing equation (10) in summation notation we have

$$\bar{F}^N = \sum_{n=1}^{N} \bar{R}_n \left\{ \lambda_n^{-1} \bar{R}_n^T \bar{G} \right\} \tag{11}$$

The essential aspect of this method is to let N take on different values and then compare the different solutions for the following equation :

$$\bar{Y}^N = \bar{F}^N * \bar{X} \tag{12}$$

That is, we choose to retain only a certain percentage of the eigenvalues of A, rejecting the smaller ones. For practical purposes, we consider only those values of N which are between

$0.2N_f$ to $0.8N_f$ where N_f is the filter length. We consider only these values since the varimax does not converge for very small N and the solution of (12) looks very similar to the original MED output for large N. When $N=N_f$, the solution of (12) is the same as the original MED solution of Wiggins (1977).

In applying the method we let N (the number of eigenvalues used in the solution) change over predetermined intervals, take the solution of (12) with the smallest N value as our reference, and plot the variance of all the other possible solutions versus N. By variance we mean here the square of the difference $(Y^* - Y^N)$, where Y^* is the solution of (12) corresponding to the smallest N value used. The advantage of such a plot is that it tells us how many possible solutions we have that are significantly different. For short filter lengths, it is probably best to plot all the output solutions Y^N and examine how those solutions change as a function of N.

EXAMPLES

The examples which follow use single channel traces. These are especially appropriate to our approach since matrix spectral decomposition is expensive computationally. For single channel problems we may write equation (6) as

$$(13) \quad \sum_{\ell} F_{\ell} \sum_{j} x_{j-\ell+1} x_{j-k+1} = U^{-1} V^{-1} \sum_{j} y_j^{*} x_{j-k+1}$$

or

$$A^{*} \cdot \bar{F} = \bar{G}^{*}$$

Since A* is now independent of Y we will have to find the spectral components of A* only once with consequent saving of computer time. The examples discussed below were constructed in such a way that a complete recovery of the generating spike sequence by the original MED version was not possible, as will be shown.

Example A.

The wavelet, spike train and the resulting trace with 2.5% added white noise is shown in Figure 1. The spacing of the spikes compared to the wavelet length makes this example a particularly difficult deconvolution problem. As stated in the last section, it is often useful to plot the variance of all possible solutions versus N. Figure 2(a) shows such a plot but

it is not of much help in this particular example because the filter length is short and the number of solution models is small.

As shown in Figure 2(b) the original version of MED was unable to recover the generating spike sequence. The spikes become increasingly visible as we reject more and more eigenvalues in the construction of the filter solution (equation (11)). Note the development of the output from Figure 2(c) to Figure 2(e). The latter does include all the input spikes shown in Figure 1(b) but it is evident that the high frequency content of the output decreases as more eigenvalues are dropped.

As shown in Chapter 3, the inverse of the MED filter is the wavelet if it is assumed that the MED output is the impulse response. We tried to recover the wavelet by finding the inverse operator of the MED filter. For this purpose we used the optimum spiking algorithm of Treitel and Robinson (1966). The results are shown in Figure 3 . The inverse of the MED filter of the original version did not give an acceptable description of the input wavelet (compare Figure 3(a) with Figure 1(a)). This result was not surprising in view of the poor spike recovery of that filter. A slight improvment was achieved by inverting the MED filter with N=8 (Figure 3(b)), but the estimated wavelet corresponding to the MED filter with N=5 is totally unacceptable even though we may consider Y^5 to be our best output (compare Figure 2(e) with 1(b)). This is easily understood in view of the clear differences in frequency content of the output sequences shown in Figures 2(e) and 1(b).

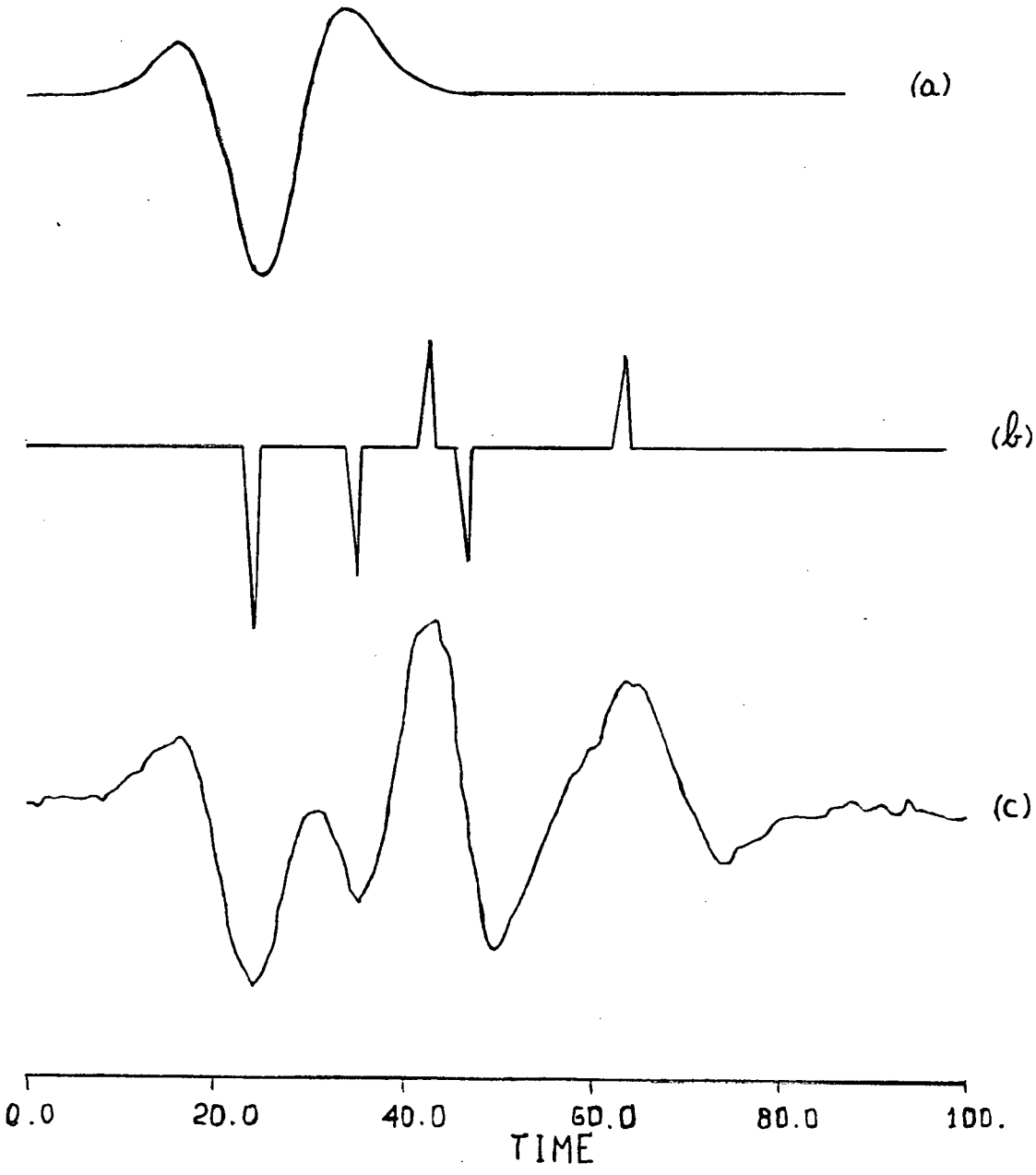

Figure 1

(a) The generating wavelet $\bar{W}$ of example A.

(b) The spike trace $\bar{S}$ from which the input trace $\bar{X}$ of example A Was derived.

(c) The input trace $\bar{X}$ that is the result of the convolution of $\bar{W}$ with $\bar{S}$ plus 2.5% White noise:

$$X = W * S + 2.5\% \text{ white noise}.$$

Figure 2

(a) A plot of the variance versus N (the number of eigenvalues used in the solution). The filter length is 14.

(b) The solution corresponding to N 14, which is identical with the original MED solution of Wiggins (1977).

(c) The solution corresponding to N 13.

(d) The solution corresponding to N 8.

(e) The solution corresponding to N 5.

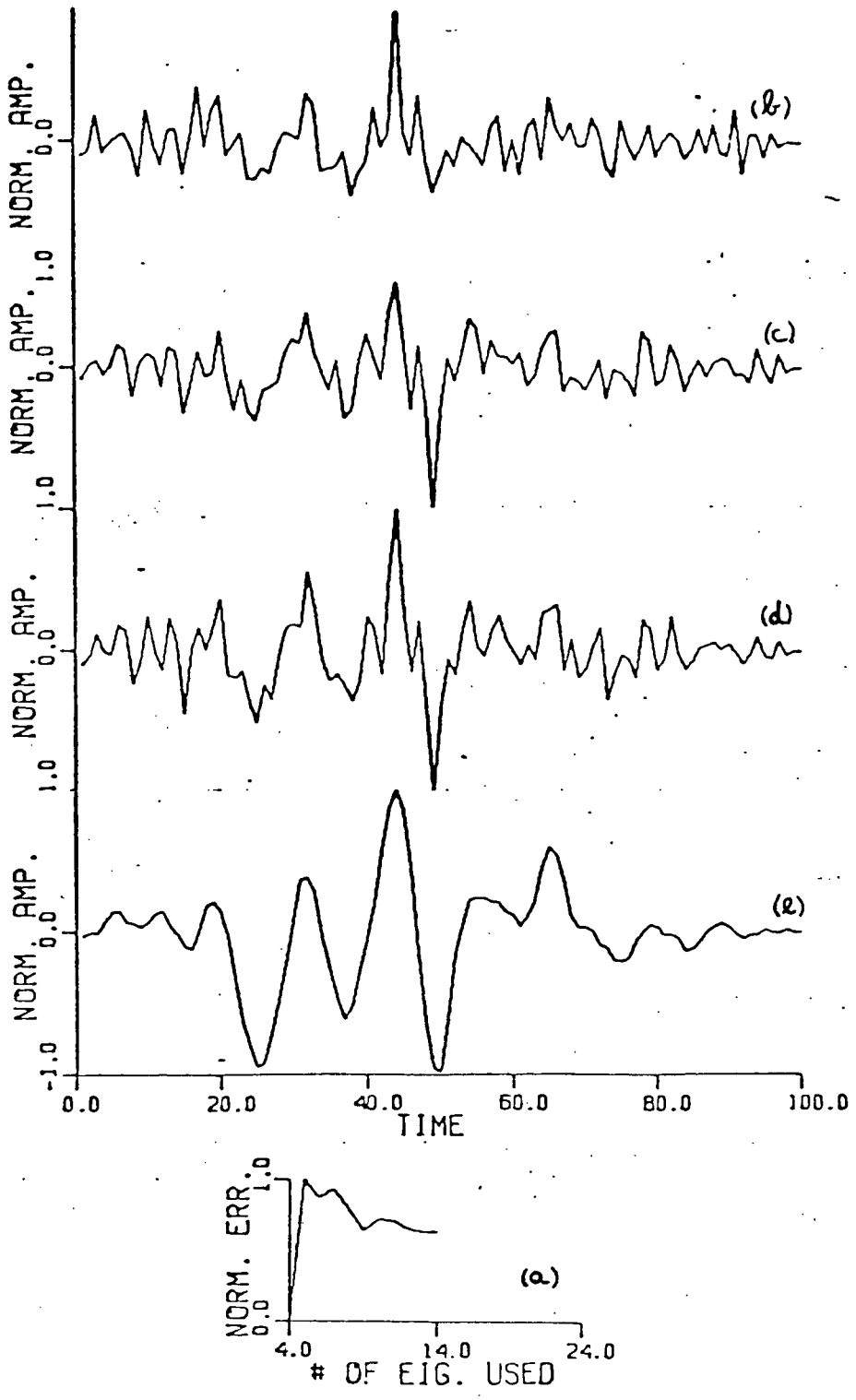
NORM. AMP.
1.0
0.0
-1.0
(b)
(c)
(d)
(e)
0.0
20.0
40.0
60.0
80.0
100.0
TIME
NORM. ERR.
1.0
0.0
(a)
4.0
14.0
24.0
OF EIG. USED

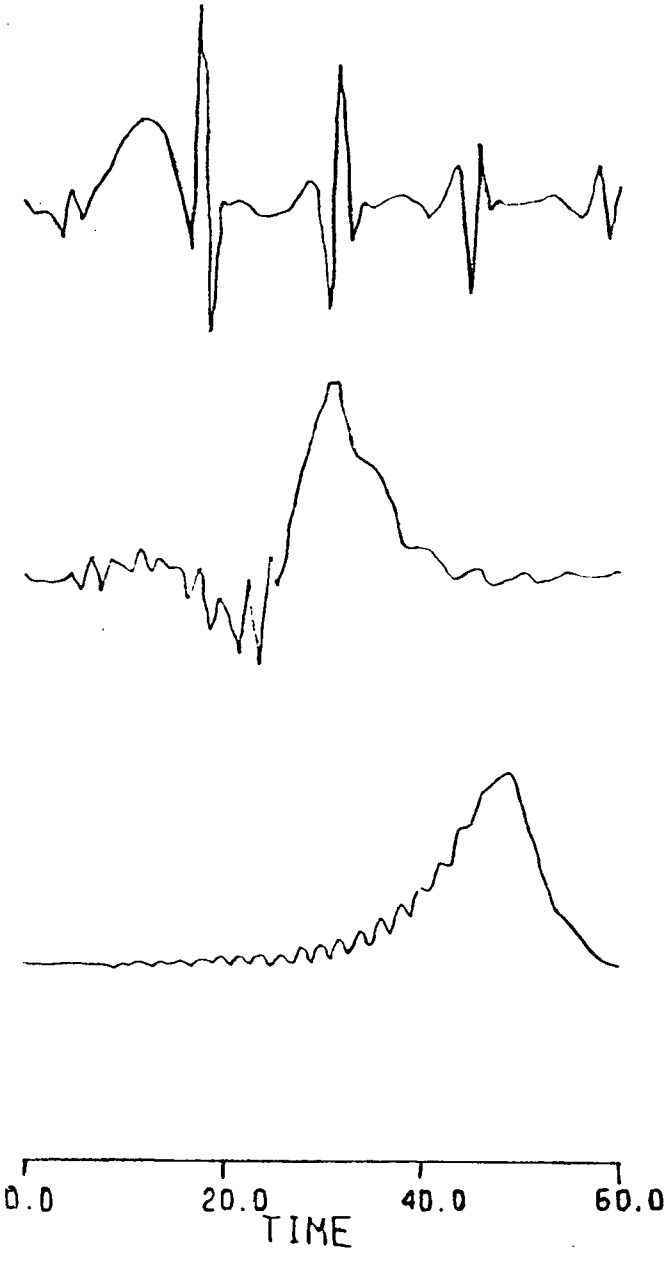

Figure 3.

(a) The inverse of the MED filter corresponding to N=14.

(b) The inverse of the MED filter corresponding to N=8.

(c) The inverse of the MED filter corresponding to N=5.

Example B.

In this example we used a somewhat more complicated wavelet (Figure 4(a)) to generate the synthetic input trace. This wavelet was convolved with the spike sequence of Figure 4(b) and 25% white noise was added. The resultant input trace is shown in Figure 4(c). Although there is wavelet overlap in this example the main obstacle is the high percentage of white ncise.

The plot of the variance versus the number of eigenvalues used in the construction of the MED filter (Figure 5(a)) proved useful in this example in which we let N take the values $N=15+2n$, $n=0,1,\ldots,30$. It is clear from the plot that there are only three significantly different sclutions to equation (12) for this example. These correspond to the flat regions between the pairs of arrows.

As shown in Figure 5(b), the original MED solution did not give a complete recovery of the generating spike sequence. However as we reject more and more eigenvalues in the construction of the MED filter a clear improvement is visible. The output Y^{29} (Figure 5(d)) does include all the generating spikes although its frequency content is much lcwer than that of the generating spike sequence, as noted before. The relative amplitudes of the recovered sequence shown in Figure 5(d), match very well with those of the input spike sequence shown in Figure 4(b).

Figure 6 shows the inverses of the filters used to derive Figures 5(b), (c) and (d). When compared with Figure 4(a), it is clear that the source wavelet was not reproduced. This is due to two causes : (1) when large numbers of eigenvalues are

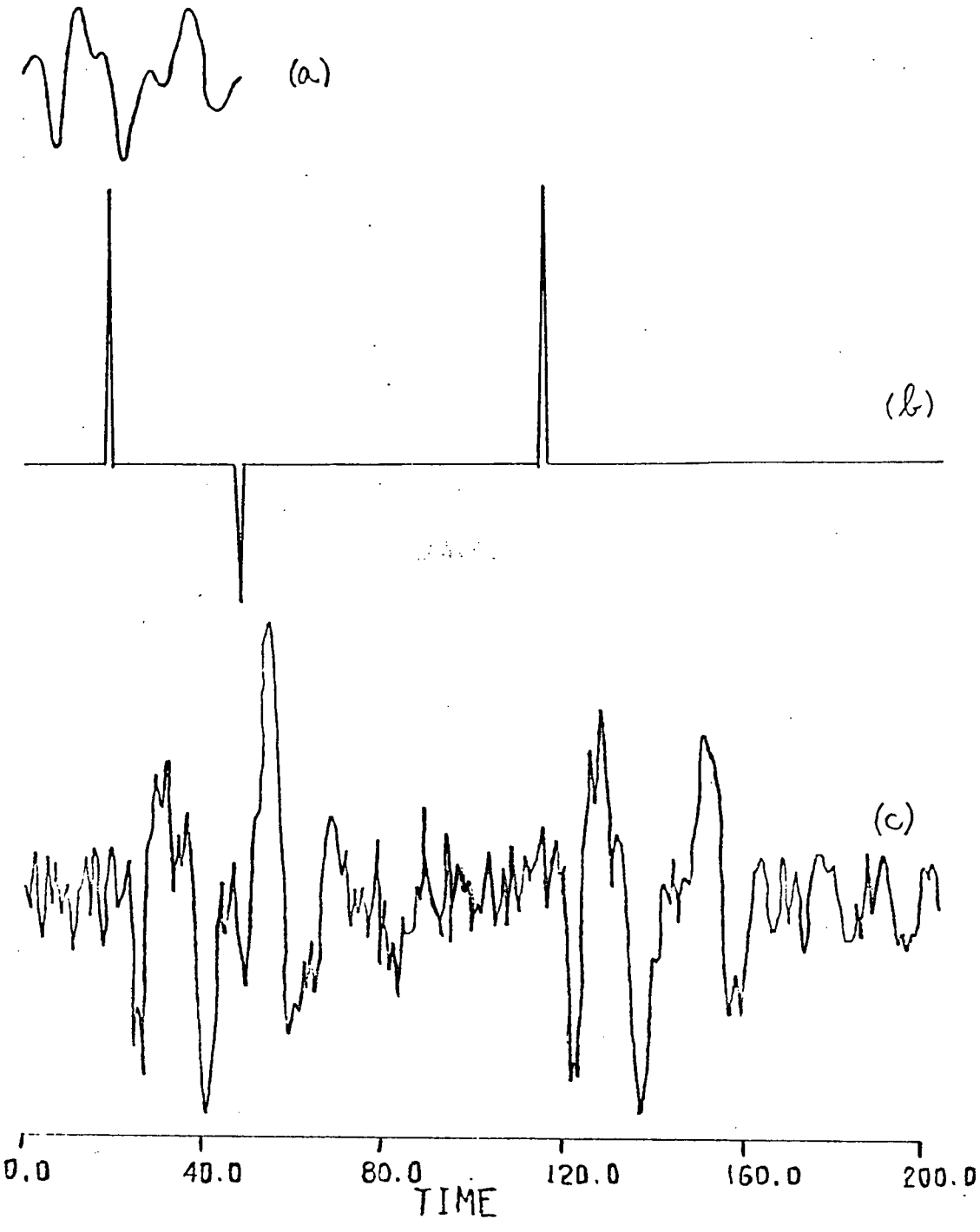

Figure 4.

(a) The input wavelet $\bar{W}$ of example B.

(b) The generating spike sequence $\bar{S}$ of example B.

(c) The input trace $\bar{X}$ i. e. the result of the convolution of $\bar{W}$ with $\bar{S}$ plus 25% white noise:

$$\bar{X}=\bar{W}*\bar{S} + 25\% \text{ white noise.}$$

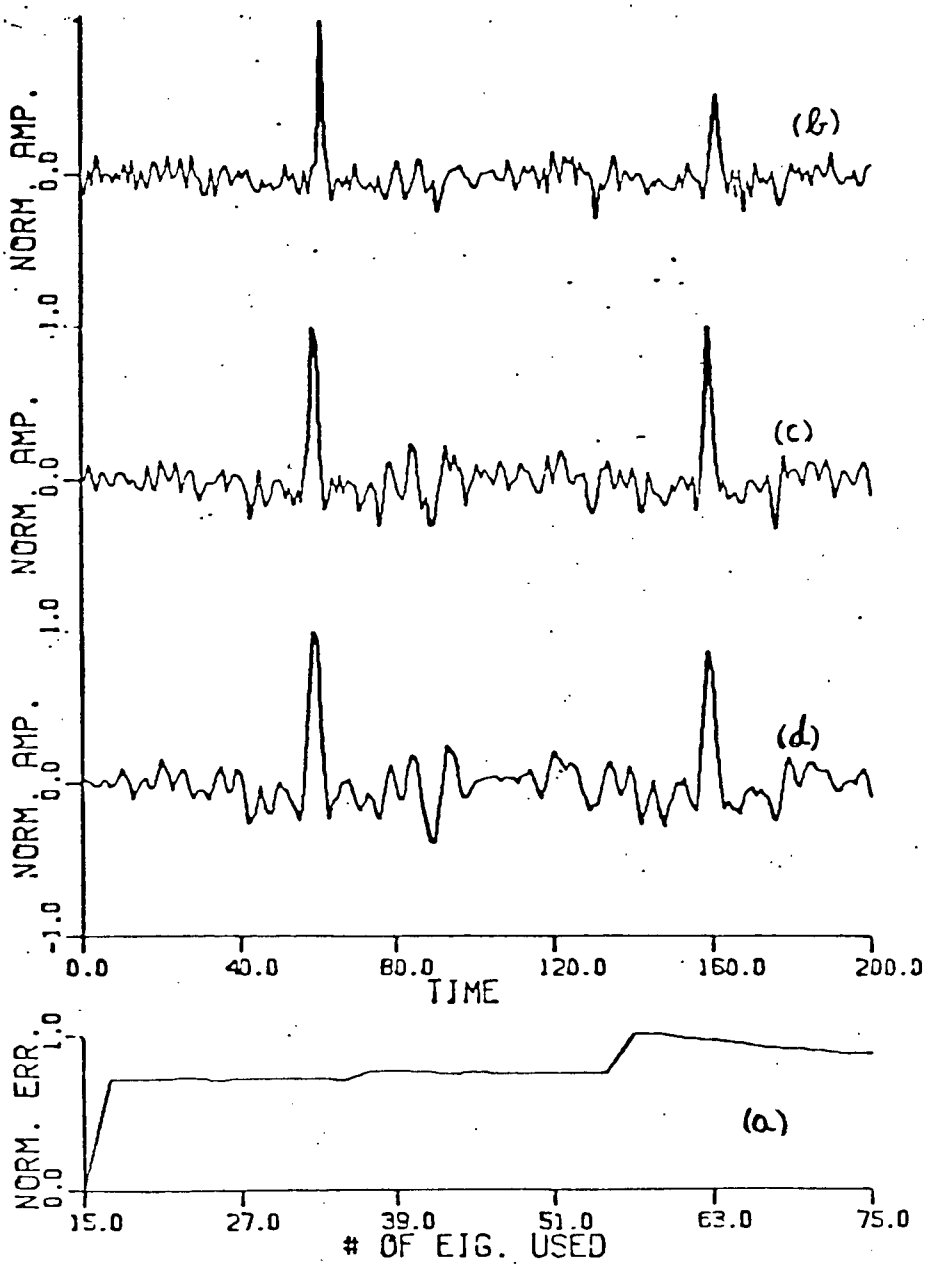

Figure 5.

(a) Variance versus N.

(b) The solution corresponding to N=75 (the original MED solution).

(c) The solution corresponding to N=49.

(d) The solution corresponding to N=29.

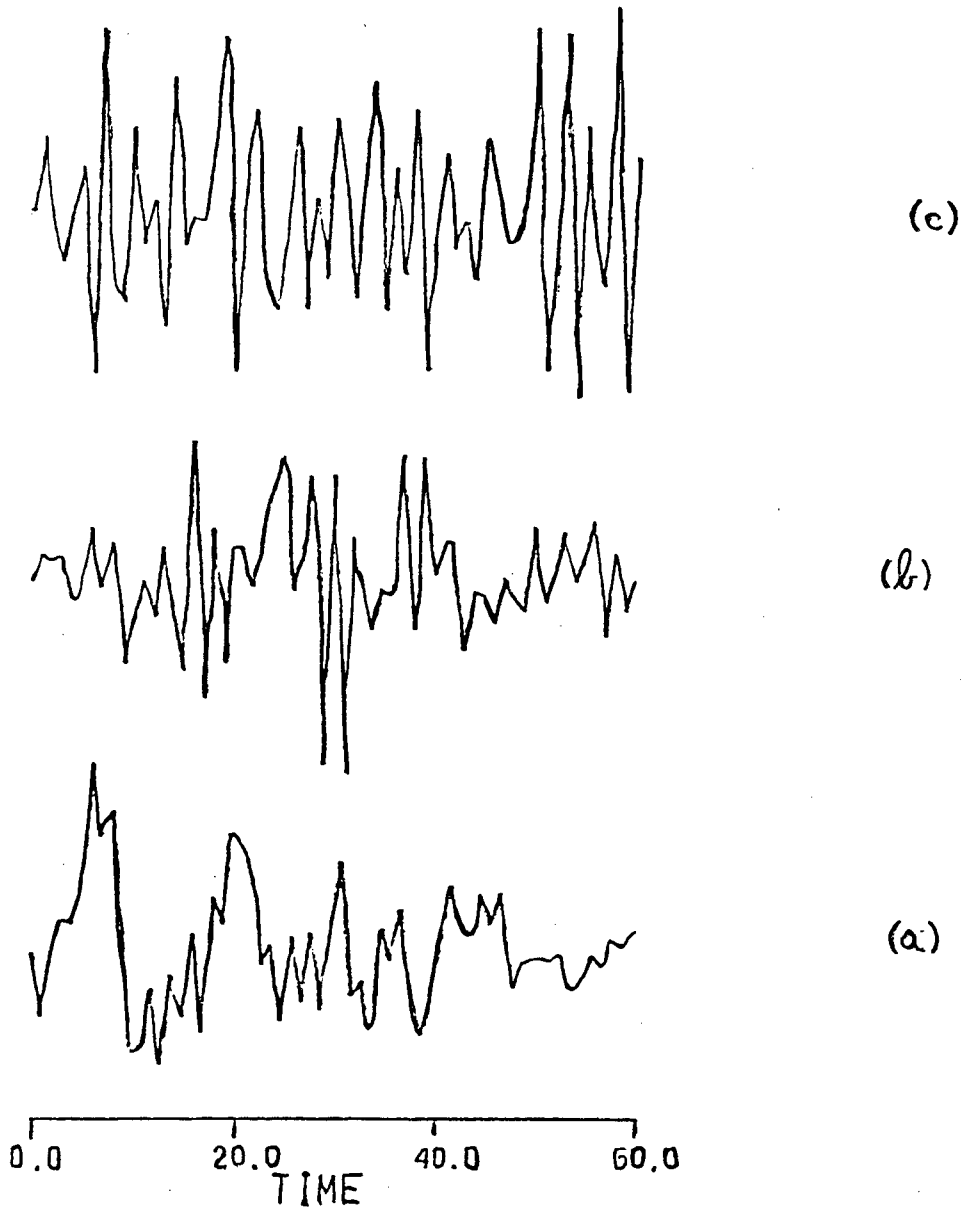

Figure 6.

(a) The inverse of $\bar{F}^{75}$.

(b) The inverse of $\bar{F}^{49}$.

(c) The inverse of $\bar{F}^{29}$.

used, the exact spike sequence has not been reproduced; and (2) when small numbers of eigenvalues are used, the frequency content of the output is much lower than that of the true spike sequence (although Figure 5(d) clearly shows the impulse response).

CONCLUSION

(a) Singular value decomposition applied to the iterative solution of the MED equations increases the signal-to-noise ratio of the deconvolved output and enhances the resolution of the MED approach.

(b) It is commonly known that those eigenvectors associated with the small eigenvalues have more zero crossings than those which are associated with the large eigenvalues (Wiggins et al 1976). Hence we expect that for a smaller N we would get a lower frequency filter F and hence the output Y will contain lower frequencies. This point is readily observed in examples A and B.

(c) The minimum value of N is determined by the varimax in the sense that for F to be an acceptable filter, the varimax must converge. Then the smallest possible N is the smallest N for which the varimax in the iterative solution described above does converge .

(d) The filter length is of essential importance in MED problems. The best filter length for our MED algorithm is the one that gives the most acceptable result in the original MED

version. An approach to this problem has recently been discussed by Ulrych et al (1979).

(e) Inversion of the MED filter resulting from our algorithm will not in general give an acceptable wavelet estimate.

CHAPTER 3

Wavelet Estimation as a Linear Inverse Problem

INTRODUCTION

The problem of wavelet estimation is one of essential importance in seismic deconvolution. It is commonly assumed that a seismogram can be modelled as the convolution of a seismic wavelet with the earth response. Since the earth response reflects the subsurface geology it is one of the main targets of seismic data processing. Given a seismic wavelet, one may deconvolve the seismogram to get the earth's response. Variations of the deconvolution problem are common in land and marine data processing. An example is the debubbling problem (Wood et al 1978) which we will treat in Chapter 4. Lines and Ulrych (1977) have summarized the current approaches to wavelet estimation. Such techniques include the Weiner-Levinson double inverse method and Wold-Kolmogorov factorization, both of which use the assumptions of an impulse response that is a white noise sequence and of a minimum phase wavelet. A more recent approach - wavelet estimation by homomorphic deconvolution - does not use these assumptions. However, it does assumes that the wavelet cepstrum is readily separable from the cepstrum of the seismic trace. (The cepstrum is defined as the inverse transform of the logarithm of the time sequence's Fourier transform.)

This work approaches the problem of wavelet estimation

using a combination of the techniques which are commonly applied in linear inversion and the method of minimum entropy deconvolution or MED (see Chapter 2). The application of MED to an input trace X will yield an output which consists of:

a. the spike sequence Y which is the primary MED output and

b. the MED filter (operator) F.

The time series represented by X, Y and F are related to each other through the following equation:

(1) $X*F=Y$

where * denotes convolution.

Figure 1 gives an example of three time series which follow the relation described in equation (1) .

By convolving both sides of equation (1) with $F^{-1}=W$, we get:

$$X*F*W=Y*W$$

or

(2) $W*Y=X$

If we assume that the time series Y is a true representation of the earth response then from equation (2), W is the wavelet. Equation (2) indicates that in order to find the wavelet we need to find the inverse of the MED operator.

One approach to doing this is to use the algorithm SPIKER given by Robinson (1967). This algorithm is designed to find the optimum inverse operator of a given time series (Treitel and Robinson 1966). It gives good results on noiseless traces as shown by Figure 1, (d) and (e).

However, the wavelet also can be estimated by formulating

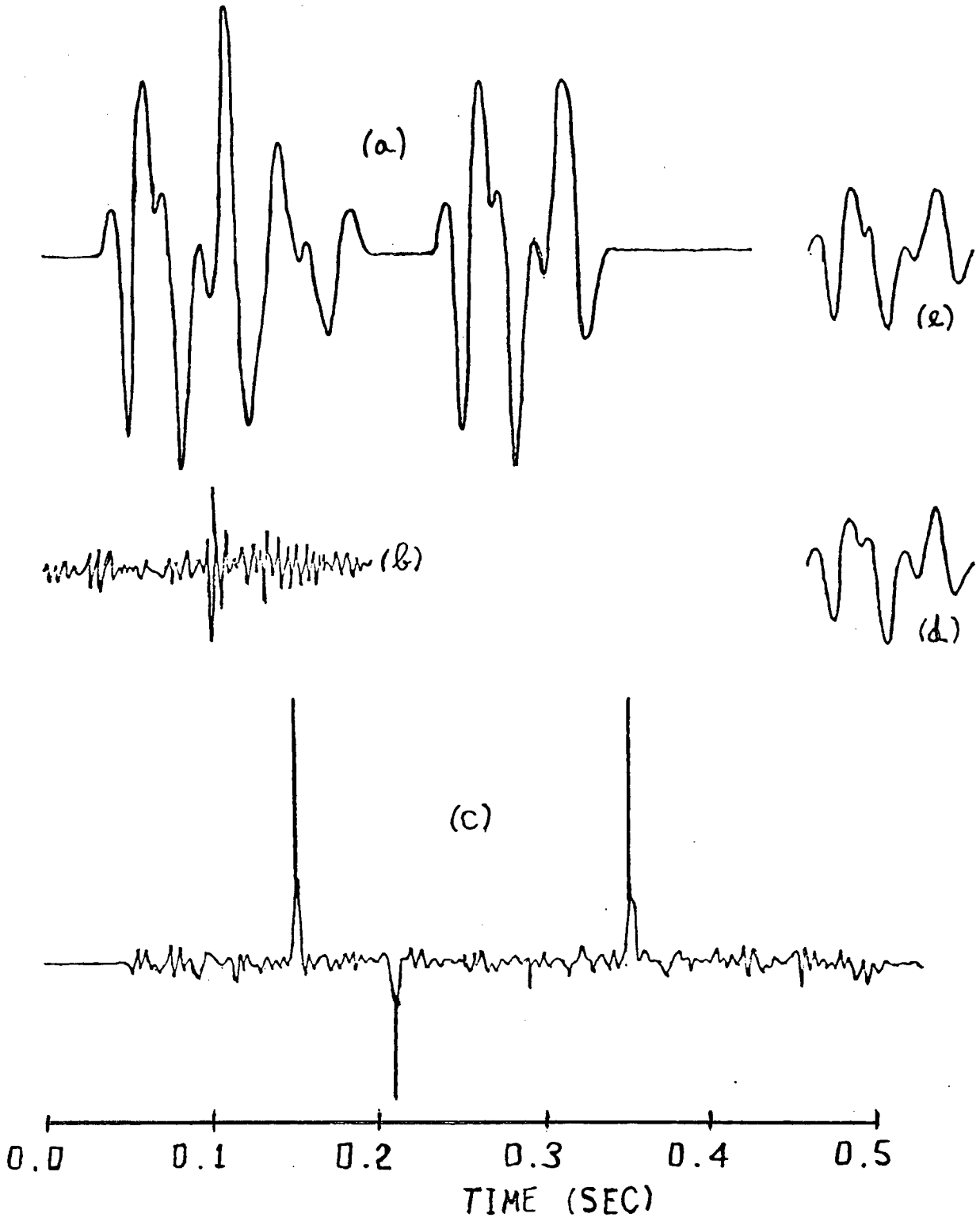

Figure 1

(a) The input trace $\bar{X}$. (b) The MED filter $\bar{F}$. (c) The spike sequence $\bar{Y}$. (d) The recovered wavelet using SPIKER. (e) The input wavelet.

equation (2) as a generalized linear inverse problem or solving the integral equivalent of equation (2) using the Backus-Gilbert approach. We assume here that the spiked minimum entropy deconvolution output is a first estimate of the earth response, and use it together with the observed seismic trace to extract the wavelet. The generalized linear inverse approach is a parametric method and the solution wavelet will be represented by a set of parameters corresponding to discrete time values. In the Backus-Gilbert approach the earth response, the observed seismic trace, and the output wavelet are all continuous functions of time . Both techniques allow the user tc control the accuracy of the solution (see the section on Practical Notes), a property which is very important when dealing with noisy data. In addition the Backus-Gilbert approach also allows us to incorporate boundary conditions into the problem.

Since we assume that the MED output represents the earth response, the quality of the estimated wavelet depends on the quality of the computed impulse response (i. e. MED output). However, we will show in example B that by using linear inverse methods a useful wavelet estimation can be extracted from seemingly useless MED output.

THEORY : CONVOLUTION AS A LINEAR INVERSE PROBLEM

A. General Linear Inverse

We will present here only those aspects of the general linear inverse theory which are relevant to our problem. For additional details concerning this approach, the reader is referred to Wiggins (1972), Jackson (1972) or Wiggins et al (1976). The generalized linear inverse development follows Wiggins et al (1976).

Writing the convolution integral in its time series form, we have:

$$(3) \qquad x_j = \sum_{k=1}^{m} w_k y_{j-k+1} \qquad j=1,\ldots,n$$

Equation (3) is a set of equations in which m unknown parameters W are related to n observations X. The matrix equivalent of (3) is

$$(4) \qquad \bar{X} = A \cdot \bar{W}$$

where $\bar{X}$ is a vector of length n which contains the observations (input trace) ; $\bar{W}$ is a vector of length m which contains the desired parameters (wavelet parameters) ; A is an nxm matrix shown in Figure 2; k is the length of the spike sequence Y; and the relation n=m+k-1 holds.

We may express the elements of A as

$$(5) \quad A(i,j) = Y(i-j+1) \qquad j=1,\ldots,m \; ; \; i=1,\ldots,n$$

with the condition that

$$A = \begin{bmatrix} Y_1 & 0 & 0 & 0 & \cdots & \cdots & 0 & 0 \\ Y_2 & Y_1 & 0 & 0 & \cdots & \cdots & 0 & 0 \\ Y_3 & Y_2 & Y_1 & 0 & \cdots & \cdots & 0 & 0 \\ \vdots & & & & & & & \\ Y_m & Y_{m-1} & Y_{m-2} & Y_{m-3} & \cdots & \cdots & Y_2 & Y_1 \\ \vdots & & & & & & & \\ Y_K & Y_{K-1} & Y_{K-2} & Y_{K-3} & & & Y_{K-m+1} & Y_{K-m} \\ 0 & Y_K & Y_{K-1} & Y_{K-2} & & & Y_{K-m+2} & Y_{K-m+1} \\ \vdots & & & & & & & \\ 0 & 0 & 0 & 0 & & & 0 & Y_K \end{bmatrix}$$

Figure 2

The input matrix A of equation (4).

$$Y(i-j+1) = 0 \quad \text{for } i-j+1 < 1 \text{ and } i-j+1 > k$$

The system in equation (3) is an overdetermined one (i.e the number of equations is larger then the number of unknowns) and it can be solved by minimizing $\overline{\Delta X}$ in a least squares sense, where $\overline{\Delta X}$ is defined by

$$(6) \quad \Delta Xi = Xi^{OBS} - Xi^{CAL} .$$

Xi^{OBS} refers to the i^{th} observation in the input vector, and Xi^{CAL} refers to the i^{th} calculated observation. Using singular value decomposition (Lanczos 1961), A is decomposed into its row and column eigenvectors and the associated eigenvalues. The generalized inverse of A is defined as (Inman et al 1973):

$$(7) \quad H_q = V_q \Lambda_q^{-1} U_q^T$$

where

U^T is the transpose of U which consists of q eigenvectors of length n associated with the column vectors of A (i.e. the data eigenvectors).

V consists of q eigenvectors of length m associated with the row vectors of A (i.e the parameter eigenvectors).

Λ^{-1} is the inverse of Λ which consists of the q eigenvalues of A in descending order. $\Lambda = \text{diag}\{\lambda_1, \lambda_2, \ldots, \lambda_q\}$; and

q is the rank of A.

The solution to equation (4) is then

$$(8) \quad \bar{W}^* = H \cdot \bar{X}$$

W* is the smallest solution (least euclidian length) that minimizes $|\Delta\bar{X}|^2$. The relation of $\bar{W}^*$ to $\bar{W}$ can be obtained by substituting equation (4) into (8) which gives

$$(9) \quad \bar{W}^* = (H \cdot A) \cdot \bar{W} = R \cdot \bar{W}$$

The matrix R is referred to as the resolution matrix (Inman et al 1973). If q=m, R is the identity matrix; but if q<m, the resolution matrix is no longer the identity matrix and $\bar{W}^*$ is a weighted summation of the parameter eigenvectors used to describe the wavelet.

The calculated observations $\bar{X}^{CAL}$ are determined from

$$(10) \quad \bar{X}^{CAL} = A \cdot \bar{W}^*$$

$\bar{W}^*$ will not be equal to $\bar{W}$ except for an ideal case ; hence the vector $\Delta\bar{X} = (\bar{X}^{OBS} - \bar{X}^{CAL})$ will not be the zero vector. As a matter of fact, in noisy cases we are not interested in reproducing the observations exactly since if we do so the

errors in the observations and/or the spike trace will propagate directly into the solution (wavelet). The power of linear inversion in this particular problem is that it gives us the ability to control the accuracy of the solution. For example, in the case of a known noise level of α % we are interested in all the models (wavelets) in which :

$$(11)\quad \text{Max}\left\{\Delta Xj\right\} \leqslant \alpha\,\% \cdot \text{Max}\left\{Xj\right\} \qquad j=1....n$$

Thus the exact solution is certainly not the only sclution that interests us and it is likely that it will not provide the best estimate of the wavelet .

B. Backus-Gilbert Inversion

The basic assumptions required for the generalized linear inverse problem - (1) MED output is a true representation of the earth response, and (2) the seismogram can be modelled as a convolution of the earth response with the input wavelet - also are applicable to the Backus-Gilbert inversion. That is, we assume that the observed seismic trace can be expressed directly by the convolution integral

$$(12)\quad X(tj) = \int_{-\infty}^{\infty} W(t) \cdot Y(tj-t) \cdot dt$$

where

X(tj) is the datum corresponding to time tj.

W(t) is the wavelet .

Y(tj-t) is the spike trace (MED output) ; Y is ccmmonly referred to as the kernel.

In the case where the functions X(t) and/or Y(t) in

equation (12) contain a certain amount of noise, we have some flexibility. Linear inverse theory allows us to choose a solution model W(t) which will reproduce the data X(t) to within a desired standard deviation instead of solving (12) exactly. This ability is the key which enables us to treat high noise problems succesfully.

Define W(t) such that :

$$W(t) = W(t) \qquad t \in (0,T)$$

$$W(t) = 0 \qquad t \notin (0,T)$$

That is, the wavelet has a finite length T. Using the definition of the wavelet we can rewrite equation (12) as

$$(13) \qquad X(Tj) = \int_0^T W(t)\ Y(Tj-t)\ dt$$

The solution to equation (13) can be constructed by minimizing either

$$(14) \qquad (W(t),W(t)) = \int_a^b (W(t))^2\ dt$$

or

$$(15) \qquad (W'(t),W'(t)) = \int_a^b (dW(t)/dt)^2\ dt$$

The solutions which we get by (14) and (15) are commonly referred to as the smallest and the flattest models, respectively. Since the flattest model discriminates against

steep gradients, we expect it will ensure good behaviour of the model in the region of interest.

1. Smallest Model

The kernels of equation (12) are generated by the MED output. Using the nomenclature Gj for the kernels we obtain

$$(16) \quad Gj(t) = Y(tj-t+1) \qquad 1 \leqslant tj-t+1 \leqslant T$$

$$Gj(t) = 0 \qquad 1 > tj-t+1 \quad \text{and} \quad tj-t+1 > T$$

Since the kernels must be at least piecewise-continuous to allow integration, it is convenient to assume that Y is constructed from a series of box cars of width Δt (otherwise a spline curve fitting approximation should be used to give a proper continuous approximation of the MED output). For example, suppose we have the MED output shown in Figure 3:

Assume the wavelet is of length 4 (T=4).

Then

$$G1(t) = Y(1-t+1) \qquad t \in (0,4)$$

$$G2(t) = Y(2-t+1) \qquad t \in (0,4)$$

$$G3(t) = Y(3-t+1) \qquad t \in (0,4)$$

$$G4(t) = Y(4-t+1) \qquad t \in (0,4) \qquad \text{etc.}$$

Figures 3 and 4 illustrate the relation between the kernels Gj and the MED output Y as specified in equation (16).

We assume that the wavelet is a linear combination of the kernels:

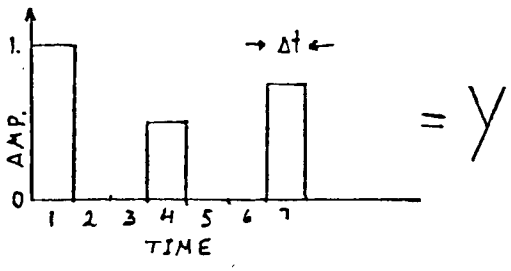

Figure 3
Example of MED output for smallest model inversion.

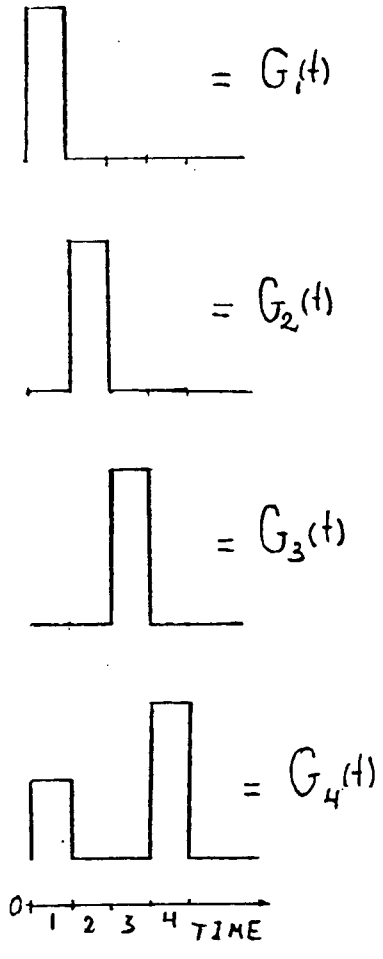

Figure 4

The kernels of the smallest model inversion generated from the MED output of Figure 3.

$$(17)\quad W(t) = \sum_{i=1}^{N} G_i(t) \cdot \beta_i$$

The coefficients β_i must be found.

Substitute (17) into (13) to get:

$$(18)\quad X(t_j) = \sum_{i=1}^{N} \beta_i \int_0^T G_i(t) \cdot G_j(t) \cdot dt$$

The problem now is reduced to the form:

$$(19)\quad \bar{X} = \Gamma \cdot \bar{\beta} \Rightarrow \bar{\beta} = \Gamma^{-1} \cdot \bar{X}$$

The inner product matrix Γ is defined by :

$$(20)\quad \Gamma_{i,j} = \int_0^T G_i(t)\, G_j(t)\, dt$$

For the above example we have

$\Gamma_{11} = 1.$

$\Gamma_{12} = 0. = \Gamma_{21}$

$\Gamma_{13} = 0. = \Gamma_{31}$

$\Gamma_{14} = 0.5 = \Gamma_{41}$ etc.

After calculating the inner product matrix, we find its spectral components which are given by the following equation :

$$(21)\quad \Gamma = R \Lambda R^T$$

where

Λ is the diagonalized eigenvalue matrix; $\Lambda = \text{diag}\{\lambda_1, \lambda_2 \ldots\}$ with $\lambda_1 > \lambda_2 > \ldots$.

R is the eigenvector matrix , and

R^T is the transpose of R.

To compute the model we use

$$(22)\quad W(t) = \bar{\beta}\cdot\bar{g}^T = (R\Lambda^{-1}R^T\bar{X})\cdot g^T \equiv \sum_{i=1}^{N} \alpha_i \psi_i(t) \;;$$

$$\bar{g}^T = (G_1, G_2, \ldots\ldots G_N)$$

ψ_i , the basis functions, and α_i , the coefficients of the basis functions, are given below .

$$(23)\quad \psi_i(t) = \frac{1}{\sqrt{\lambda_i}} \sum_{j=1}^{N} R_{ji}\, G_j(t)$$

and

$$(24)\quad \alpha_i = \frac{1}{\sqrt{\lambda_i}} \sum_{j=1}^{N} R_{ji}\, X_j$$

Since the kernels can be described by a sum of step functions the model also will be a sum of step functions .

2. Flattest Model

To derive the "flattest" model, the kernels (the MED output Y) are assumed to be a series of δ functions . In this case, equation (16) takes the form:

$$(16a)\quad G_j(t) = y(t_j - t) \sum_{n=1}^{N} \delta(t - n\Delta t) \qquad 0 \le t_j - t \le T$$

$$= 0 \qquad\qquad 0 > t_j - t \text{ and } t_j - t > T$$

Δt is the digitization interval of the MED output. Note the

difference in the spike sequence representation. Here we use a δ function rather then the step function used in the smallest model case. Integrating equation (15) by parts we get

$$(25) \qquad X(Tj) = Hj(t) \cdot W(t) \Big|_0^T - \int_0^T Hj(t) \cdot W'(t) \cdot dt$$

where

$$(26) \qquad Hj(t) = \int_0^T Gj(t) \cdot dt \qquad ; \qquad W' = dW/dt$$

By the boundary conditions imposed by physical considerations, $W(0) = W(T) = 0$, we have

$$Hj(t) \cdot W(t) \Big|_0^T = 0$$

and the new integral equation is

$$(27) \qquad -X(Tj) = \int_0^T Hj(t)\ W'(t)\ dt$$

We proceed by solving equation (27) exactly as we did in the smallest model case except for the different representation of the kernels.

A simple example may help to clarify the technique. Suppose that we have the same MED output as before and assume that the wavelet length is now T=5 (change of wavelet length is needed because of the different kernel representation). Then the MED output Y, the first four functions Gj(t) (j=1..4) and the corresponding new kernels Hj(t) are shown in Figure 5.
We have made use of the fact that

$$(28) \qquad \int_{-\infty}^{\infty} \delta(t)\, dt = 1$$

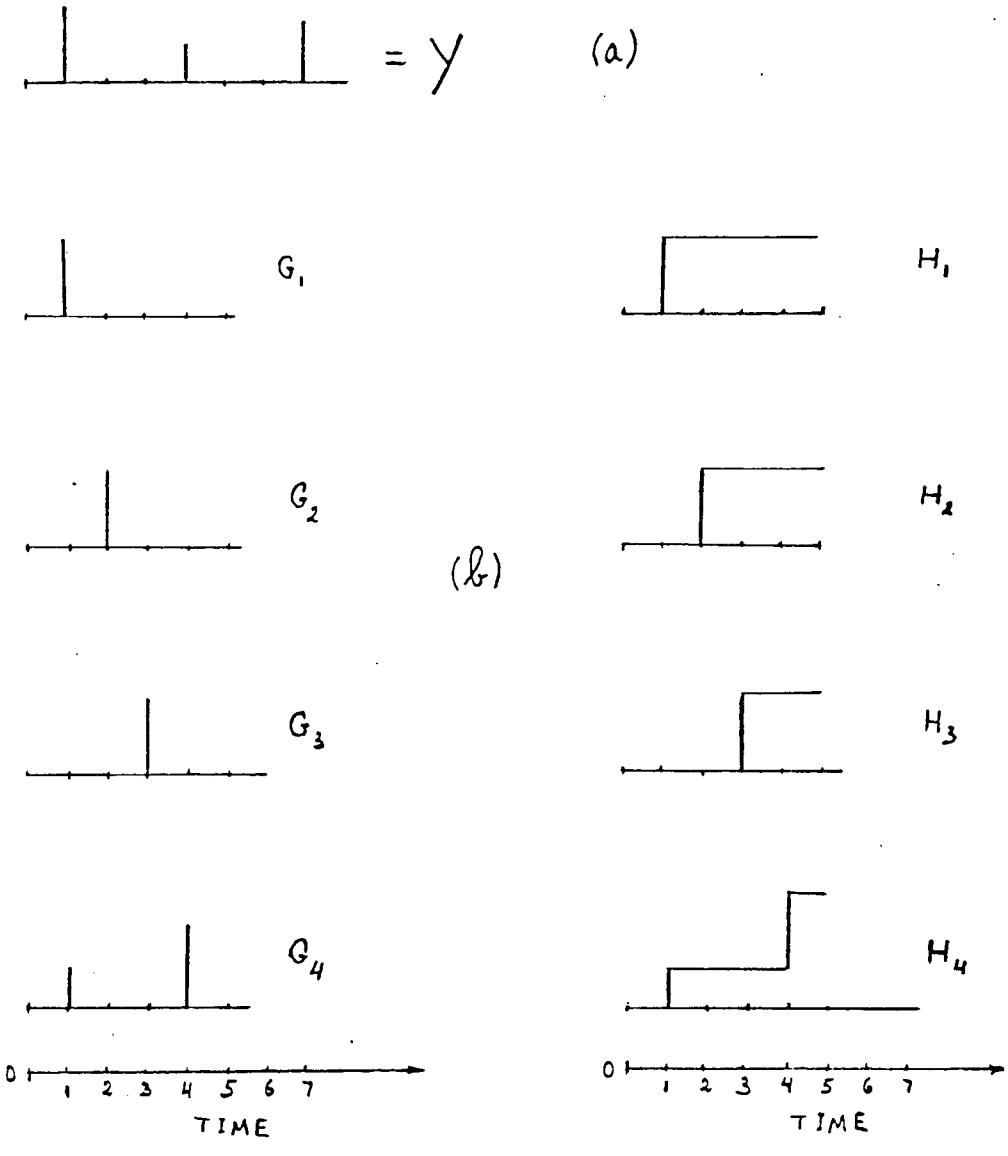

Figure 5

(a) An example of the delta function representation of the MED output Y as was used in the flattest model inversion.

(b) the smallest model kernels G generated from the spike sequence Y shown in (a) and the corresponding flattest model kernels H (G relate to Y through equation 16(a), and H relate to G through equation (26)).

Again we compute the inner product matrix by

$$\Gamma_{i,j} = \int_0^T H_i(t) \cdot H_j(t) \cdot dt \qquad (29)$$

For the above example we have:

$\Gamma_{11} = 5.$

$\Gamma_{12} = 4. = \Gamma_{21}$

$\Gamma_{13} = 2. = \Gamma_{31}$

$\Gamma_{14} = 3. = \Gamma_{41}$ etc.

Having the inner product matrix we proceed to find its spectral components which are defined by equation (21). Writing the solution in terms of the coefficients α_i and the base functions ψ_i and integrating to get the wavelet model we have:

$$W(t) = \int_0^t w'(t)\, dt' = \text{CONSTANT} + \int_0^t \left(\sum_i \alpha_i \psi_i(t') \right) dt'$$

where the constant of integration is defined by the boundary conditions. ψ_i , the base functions, and α_i , the coefficients of the base functions, are defined by equations (23) and (24), respectively (with H replacing G).

C. Practical Notes

(a) The MED output might have a polarity which is the reverse of the real spike sequence and hence the wavelet polarity might also be reversed (Wiggins 1977).

(b) The wavelet is represented by the following expressions :

1. Generalized linear inverse

$$\bar{W}^* = V_g \Lambda_g^{-1} U_g^T \cdot \bar{X}$$

or following Wiggins et al (1976)

$$\bar{W}^* = \sum_{k=1}^{Q} \bar{V}_k \left(\bar{U}_k^T \lambda_k^{-1} \cdot \bar{X} \right) \tag{30}$$

2. Backus-Gilbert inversion

$$W^*(t) = \sum_{i=1}^{N} \alpha_i \psi_i(t) \tag{31}$$

What we are actually looking at are the different models W* corresponding to different values of Q in the generalized linear inverse approach or N for the Backus-Gilbert inversion.

(c) Since there are Q^0 models which can be generated by the generalized linear inverse method and N^0 models which can be generated by the Backus-Gilbert inversion (Q^0 is the rank of A and N^0 is the rank of Γ), we will have to analyse many models. Fortunately those models can be grouped into a small number of groups. The following methods enable a grouping

of the models without the necessity of examining every one of them.

1. Generalized linear inverse:

A plot of (Q^0-Q) versus $\max\{|\Delta x_i|\}$ (Q^0 is the rank of matrix A), has an en echelon like shape and allows an easy detection of the groups. The en echelon shape can be explained by equation (30) which states that the solution model is a linear combination of the parameter eigenvectors. It is commcnly known that the more "reliable" contributions to the solution come from those eigenvectors associated with the larger eigenvalues. Summation of these contributions forms the large amplitude part of the signal. Removal of those eigenvectors which are associated with the smaller eigenvalues will not change significantly the shape of the derived signal.

2. Backus-Gilbert inversion

A plot of (N^0-N) versus standard deviation also has an en echelon shape (N^0 is the rank of the inner product matrix).

(d) All the models are multiplied by a cosine bell to ensure zero values at both ends.

(e) For good quality MED output we expect the best models to be those that use Q^1 and N^1 terms in the summations (30) and (31) respectively, since these include all the reliable contributions in the solution. Q^1 is the practical rank of A in the generalized linear inverse and N^1 is the practical rank of the inner product matrix Γ in the Backus-Gilbert inversion. The practical rank is determined by the number of eigenvalues which satisfy the following condition

$$\frac{\lambda i}{\lambda_{max}} \geq \text{RATIO} .$$

For double precision computer calculations we take RATIO to be 10^{-10}.

EXAMPLES

Example A (Good quality MED output)

The input trace X shown in Figure 6(a) is a result of the convolution of the wavelet shown in Figure 6(c) and the spike sequence of Figure 6(b). This trace has been convolved with the MED filter and the resultant spike trace Y^0 is shown in Figure 7. The spike trace Y^0 was truncated from both sides so that its length will follow the relation "length of observations = length of spike sequence + length of wavelet - 1" and the resultant trace is the spike sequence Y chosen as the part of the trace between the arrows in Figure 7. Truncation is based on interpretation of the numerical values of the trace Y^0. In this example it is clear where Y^0 should be truncated, since it is desirable that the spike signal includes the larger spikes of the MED output. Note that Y (the truncated trace) includes only the section of Y^0 that contains the major spikes. That is, the interpretation has assumed that small amplitude 'bumps' are noise and can be rejected.

Using the inversion schemes described previously, with the input X and Y as specified above, we get the results shown in Figure 8. The inverse operator of the MED filter (Figure

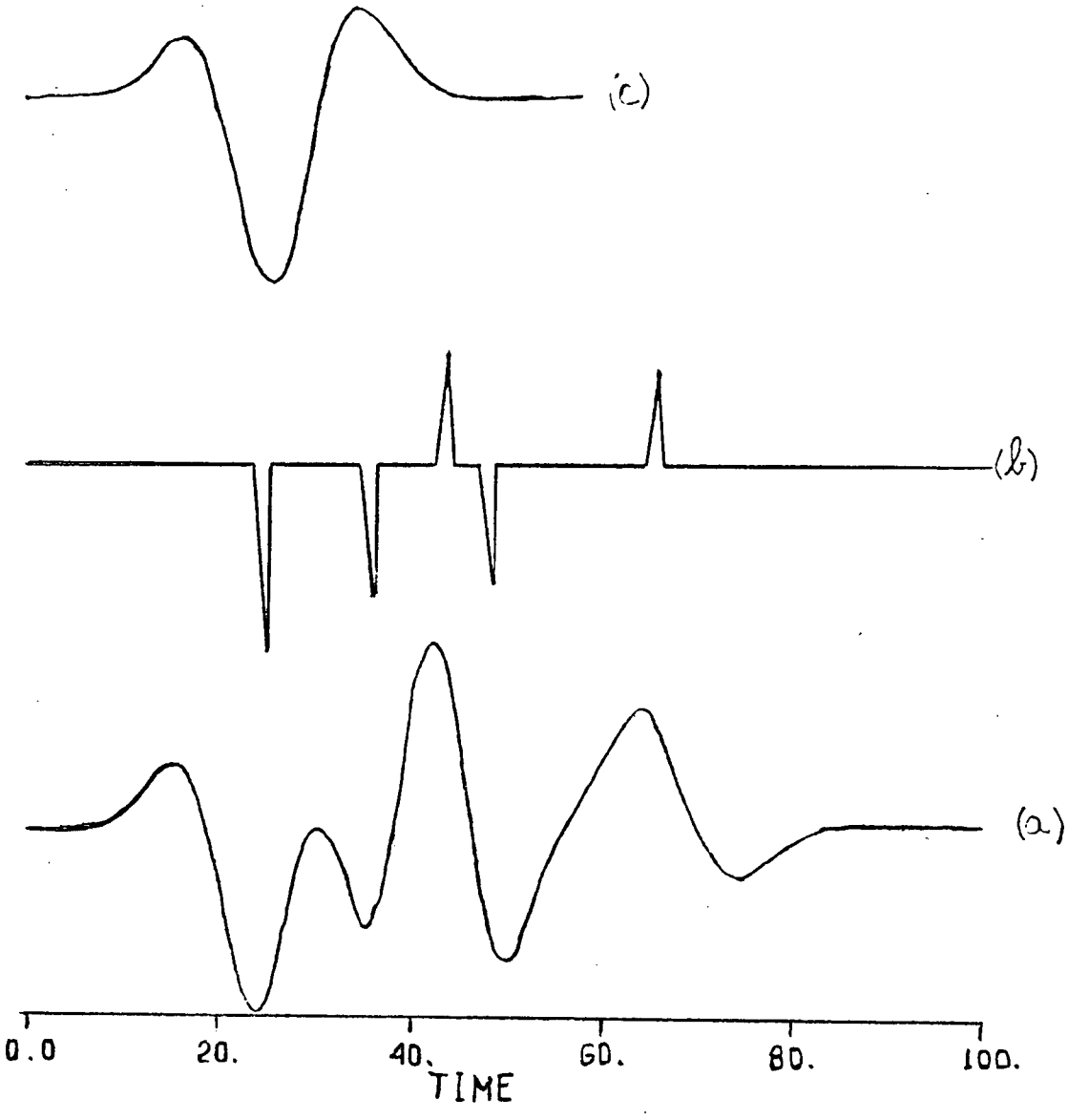

Figure 6

(a) The input trace X which is the convolution of the spike sequence shown in (b) with the source wavelet shown in (c).

(b) The generating spike sequence.

(c) The source wavelet.

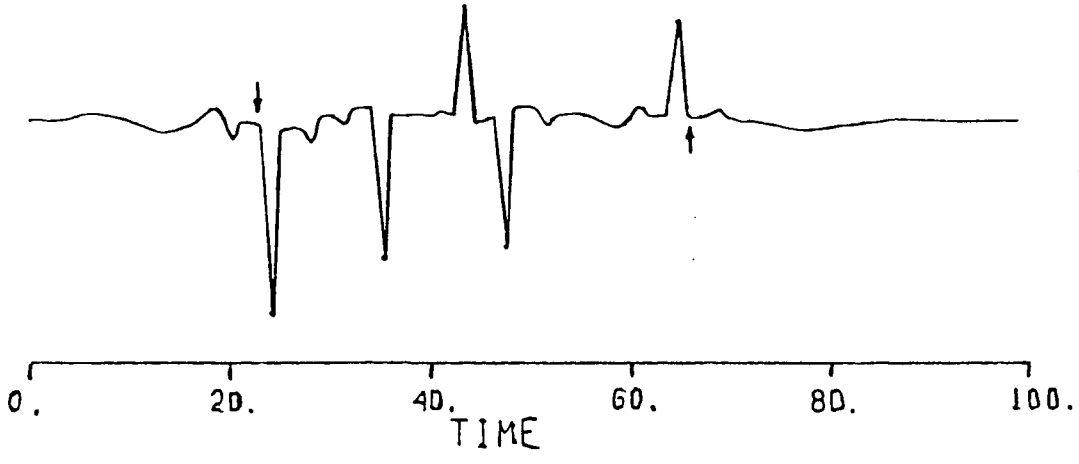

Figure 7

The MED output Y. That is, the result of the convolution of the MED filter with trace X of Figure 6(a). Arrows mark the section Y used in the inversion schemes.

8(d)) is an acceptable description of the generating wavelet although its side lobes are exaggerated. This wavelet estimation is limited in the sense that errors in the MED filter propagate directly into the estimated wavelet. The solution wavelet of the smallest model scheme, Figure 8(c), does show the general features of the generating wavelet, but it also includes an unacceptable amount of noise (oscillatory parts in both ends of the recovered signal). The flattest model and the generalized linear inverse solutions Figure 8(b) and (a), are good descriptions of the generating wavelet shown in Figure

6(c).

Except for polarity reversals, which result from polarity reversal of the MED output, the estimated wavelets shown in Figure 8 are acceptable descriptions of the source wavelet. However, the correct amplitude relation of the small lobes which precede and follow the large amplitude part of the signal has been lost. The deviation of the estimated wavelets from the generating wavelet is a result of the small numerical noise that contaminates the estimated spike sequence (the MED output). As mentioned in the section Practical Notes, paragraph (e), we expect to get the best results when Q^1 and N^1 assume the value 59, the assumed length of the wavelet. The generalized linear inverse model (Figure 8(a)), and the flattest model (Figure 8(b)), behaved in this manner but the smallest model (Figure 8(c)) did not. It is possible that either the smallest model scheme is more sensitive to noise or that the box car representation of the kernels is inadequate, or both.

The spike trace can be treated further by setting

$$(32)\qquad y_j = \begin{cases} y_j & \text{for } |y_j| \geq 0.1 \\ 0 & \text{for } |y_j| < 0.1 \end{cases}$$

This specification is justified by the assumption that the small values in the MED output are actually noise which has been generated by the MED algorithm. The validity of this assumption can be checked by synthetic examples. Comparison of Figure 6(b)

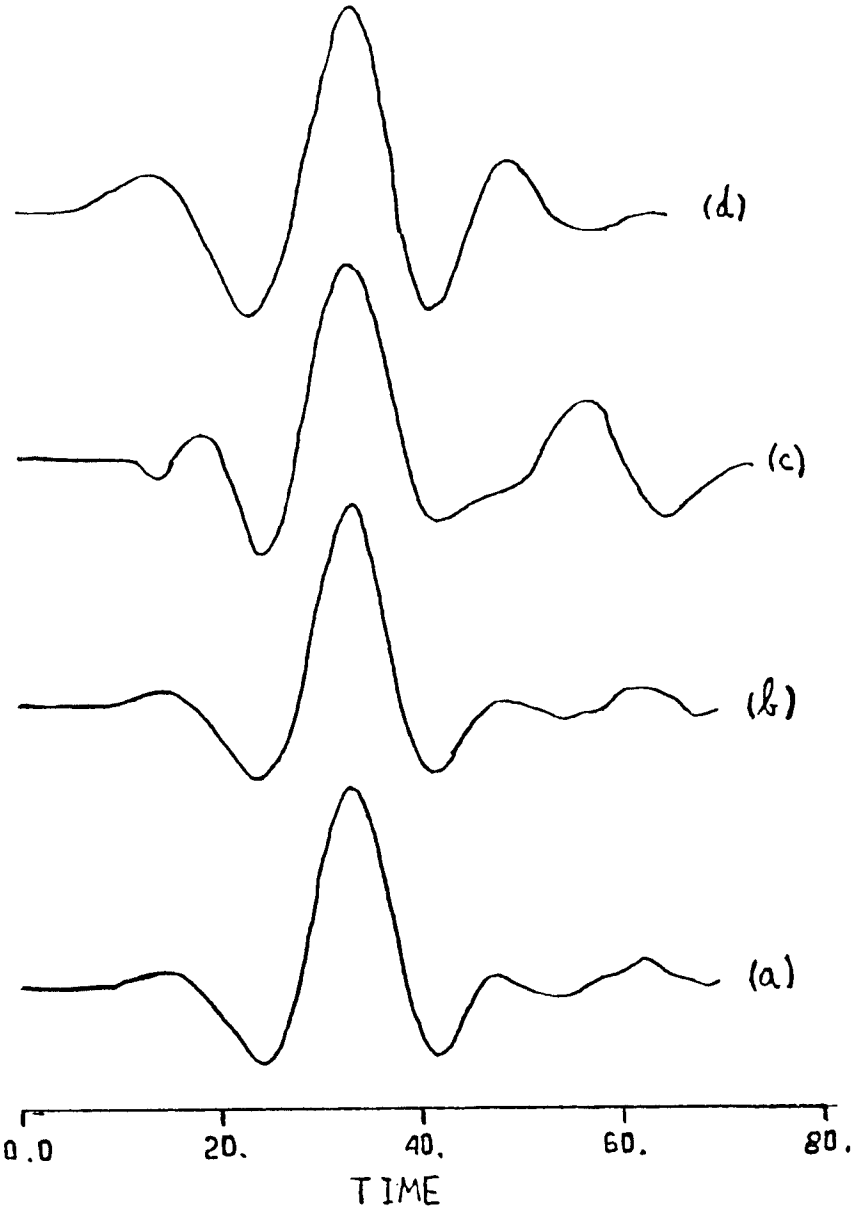

Figure 8

(a) The estimated wavelet using general linear inverse approach

(b) the estimated wavelet using the flattest model (N=59).

(c) the smallest model wavelet with N=10.

(d) The wavelet produced by inverting the MED filter.

Note that the derived wavelets have reversed polarity compared with the input wavelet of Figure 6(c) (see Practical Notes (a)).

with Figure 7 shows that the MED output does include some small 'bumps' which were not included in the generating spike sequence. Equation (32) excludes those 'bumps' from the input spike sequence Y.

The spike trace Y as defined in equation (32) and trace X of Figure 6(a) are processed with the inversion procedures. The results are shown in Figure 9. The smallest model wavelet Figure 9(a) does not reproduce the source wavelet to within the expected standard. For this reason, we will not show additicnal examples using the smallest model calculations. Note that the models of Figure 9(b) and (c) reproduce the original wavelet very well.

The exact reproduction of the input wavelet by the flattest model (Figure 9(b)), and the generalized linear inverse model (Figure 9(c)), is expected, since in this particular example equation (32) converts the problem to an almost noiseless one.

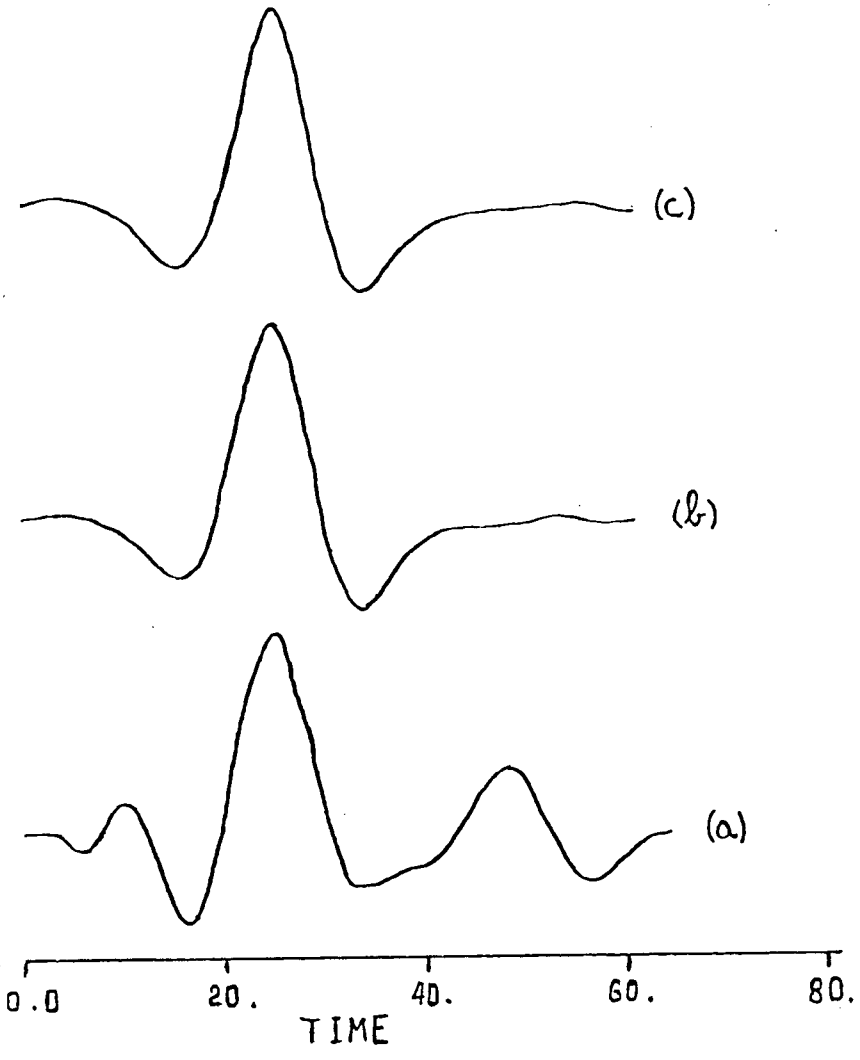

Figure 9

(a) The smallest model wavelet (with N=10).

(b) the flattest model wavelet (with N=59).

(c) the general linear inverse model wavelet (with Q=60).

Example B (Low quality MED output)

This example was designed to demonstrate the performance of the different approaches in cases of low quality spike traces. We will show that the linear inversion schemes are capable of extracting useful information out of seemingly meaningless spike traces.

In Figure 10(a) and (b) we show the input trace X, basically the one shown in Figure 6(a) plus 2.5 % white noise, and the "spike" trace Y^0 which is the result of the convolution of the MED filter with X. In this case, the MED operator failed to fulfill its function of simplifying the observations and deriving the correct spike sequence. Compare Figure 10(b) to Figure 6(b), the latter showing the spike sequence that has been used to generate this example.

First Y^0 is truncated to obtain Y (the arrows in Figure 10(b) mark the truncation). In this example, it is not easy to determine which part of Y^0 should be used and we simply choose Y to be that section of Y^0 which includes the large spike at its center. Traces X and Y described above form the input for the inversion schemes. The results are shown in Figure 12 and 13.

Since the spike input trace in this example is of low quality (i. e. contaminated by errors), we don't expect that the model that will give the smallest standard deviation will be our best model. In fact, the model which will reproduce the observations exactly will necessarily include erroneous components which are due to the errors in the spike sequence. In order to decrease the weight of the errors in the spike

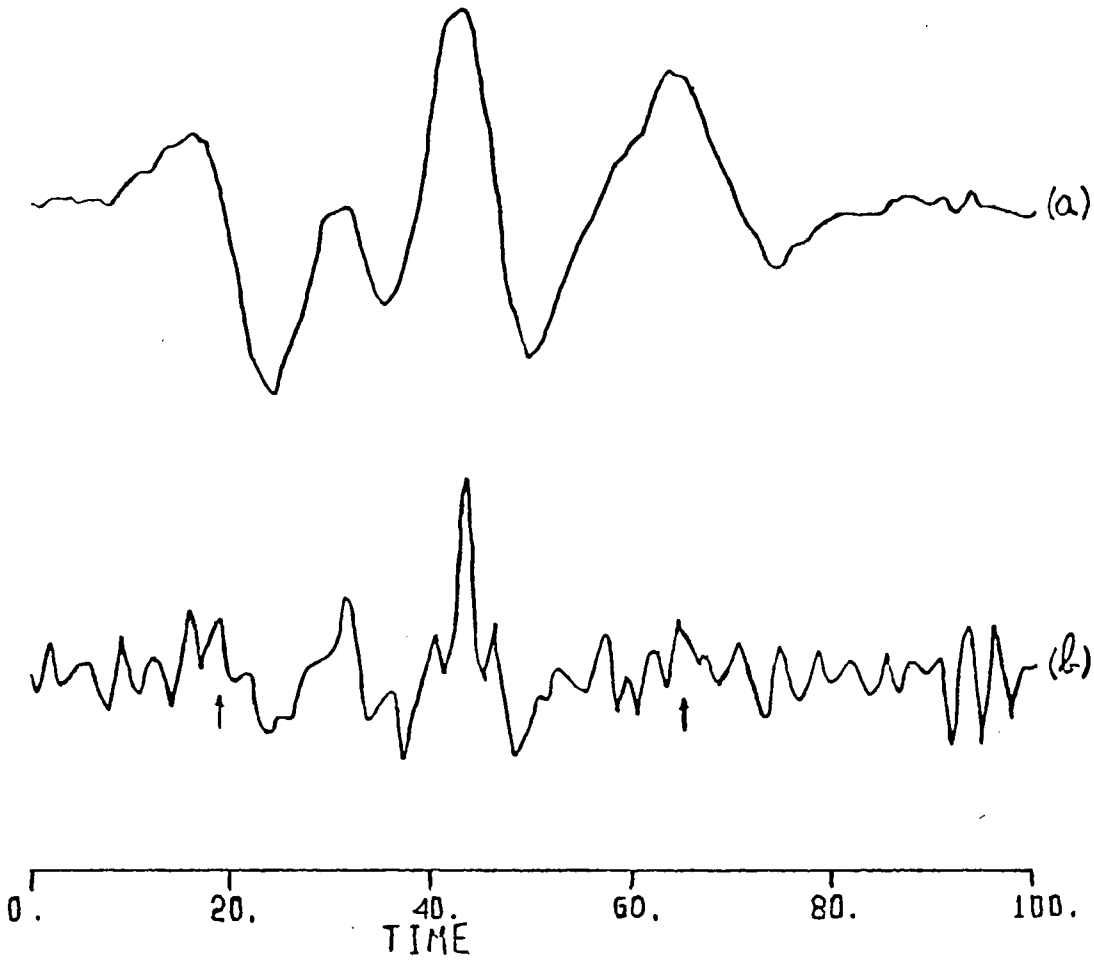

Figure 10

(a) The input trace X of example B. This trace is basically the one shown in Figure 6(a) plus 2.5% white noise.

(b) The MED output Y° used in example B. This trace is the convolution of the trace in (a) and the MED filter. Arrows mark the section used in the inversion.

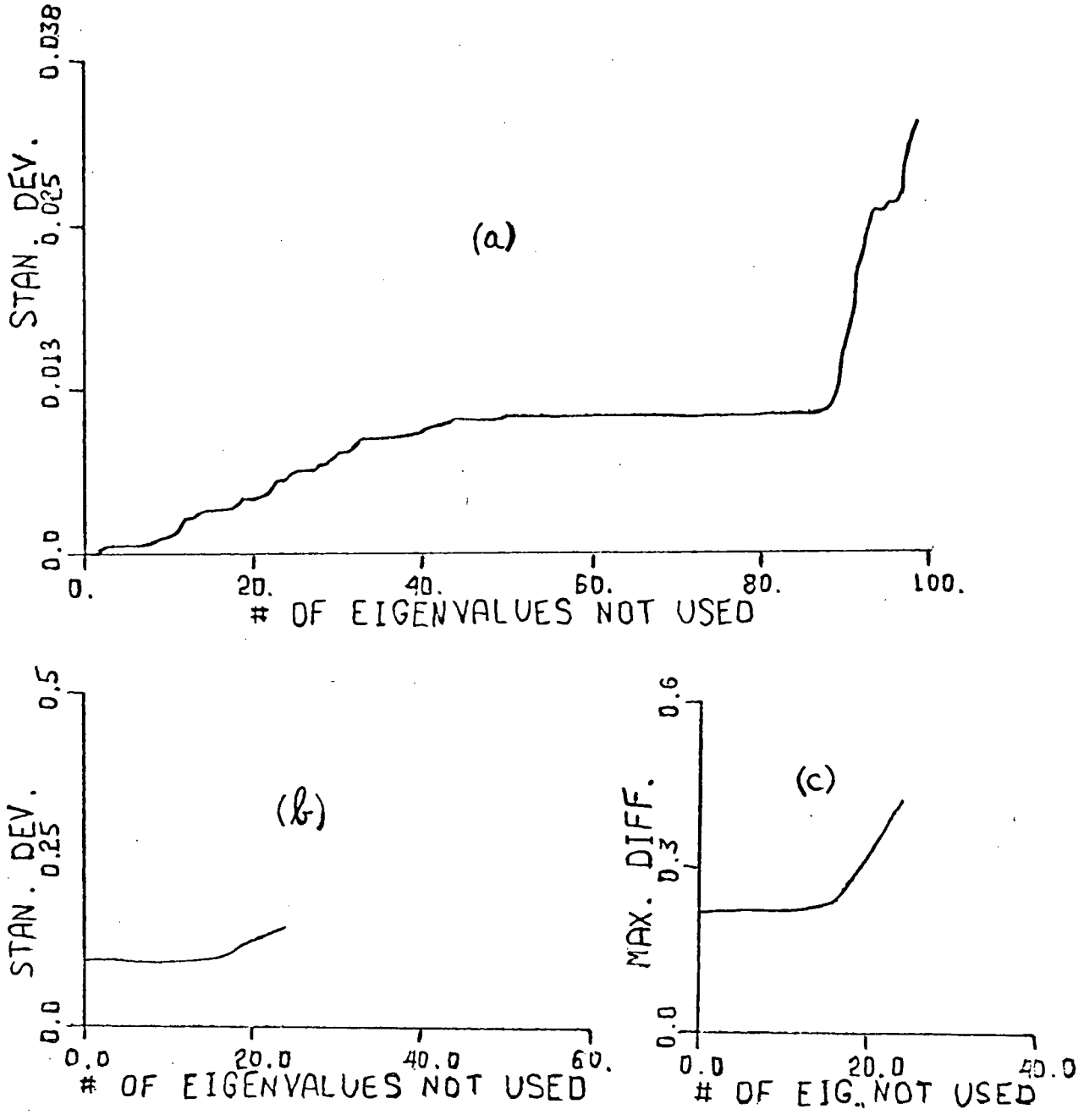

Figure 11

(a) A plot of standard deviation versus (N^0-N) for the flattest model.

(b) A plot of standard deviation versus (Q^0-Q) for the general linear inverse problem.*

(c) A plot of (Q^0-Q) versus $\text{Max}\{|\Delta x_i|\}$ shows the same general behavior as is noticed in (b).

sequence we have to allow some 'errors' in the reproduced observations. Hence we will have to use the plots of standard deviation, and maximum error, in order to analyse the different possible models (see section Practical Notes, paragraph (c)). In Figure 11(a), the standard deviation for the flattest model versus (N^0-N) is plotted. In this example N^1 (practical rank of Γ) is 55. Note the flat region corresponding to $45<N^0-N<90$. The significance of this region is that all models in which $10<N<55$ reproduce the observations to within the same standard deviation and hence they can be represented by two models, one for each end of this region.

A plot of the standard deviation and the maximum error versus Q^0-Q (Figures 11(b) and (c)) for the generalized linear inverse model shows a flat region corresponding to $Q^0-Q<16$. Here we will represent all those models in which $40<Q<56$ by one model, corresponding to the center of this flat region.

The solution wavelets that represent the different groups are shown in Figure 12 for the generalized linear inverse and Figure 13 for the flattest model solutions. Note the similarity in the general features of the different models. The flattest model solution corresponding to N=10 (Figure 13(b)) is the best estimated wavelet. This is an excellent estimation considering the quality of the input spike sequence. Compare Figures 13(b) and 6(c), and consider the fact that we used the spike sequence shown in Figure 10(b) which poorly resembles the true spike sequence of Figure 6(b).

Note that the large amplitude part of the signal does not change much from one model to another. This type of behavior

has been discussed in the Practical Notes, paragraph (c).

Example C (Synthetic seismogram)

In the following example we will show that the assumption that a seismogram can be modelled as the convolution of a wavelet with the earth's response where the response function is represented by the MED output, is useable. This assumption enables a representative wavelet to be computed.

A synthetic seismogram using generalized ray theory (Wiggins and Helmberger 1974) has been computed from the model shown in Figure 14. The following rays were considered :

1. Leaving the source as a P wave and received as a P wave ; arrival time 0.745 sec; relative amplitude 0.33.

2. Leaving the source as P and received as S ; arrival time 0.928 sec for the reflected energy and 0.927 sec for the refracted energy; relative amplitude for the combined response is 0.385.

3. Leaving the source as a S wave and received as S ; arrival time 1.119 sec; relative amplitude 1.0.

4. Leaving the source as P, reflecting from surface B, reflecting from surface A, bouncing again from surface B and received as P ; arrival time 1.374 sec; relative amplitude 0.09.

Figure 15(a) shows the synthetic trace computed from these ray paths. The model was constructed such that it will show strong interference. In such a case, the MED algorithm cannot

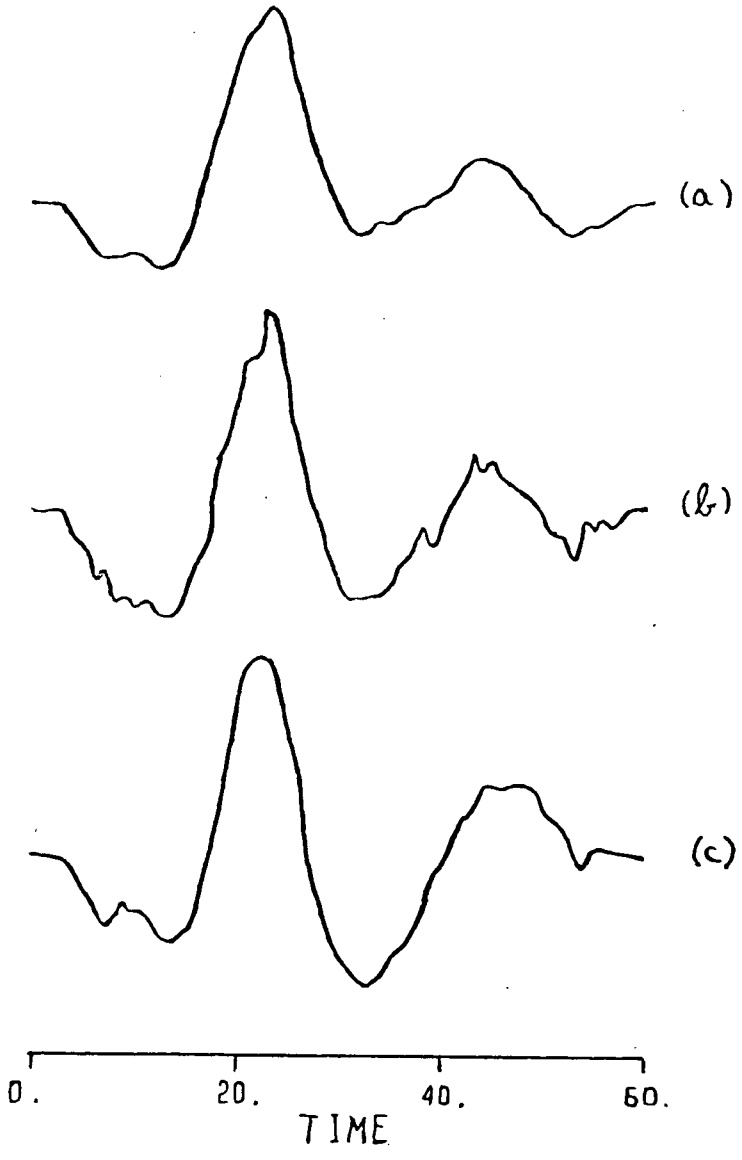

Figure 12

The results of the general linear inversion:

(a) The model corresponds to Q=44 (Q^0-Q=12), standard deviation=0.1 and Max $\{|\Delta X_i|\}$ =0.22.

(b) The model corresponds to Q= 36 (Q^0-Q=20), standard deviation=0.13 and Max $\{|\Delta X_i|\}$ =0.32.

(c) The model corresponding to Q=32 (Q^0-Q=24), standard deviation=0.15 and Max $\{|\Delta X_i|\}$ =0.42.

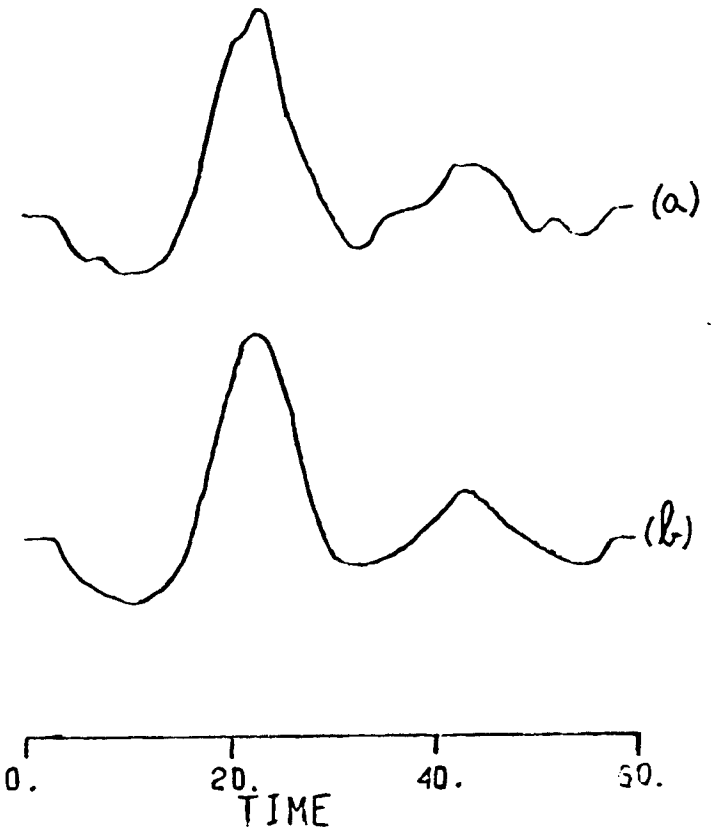

Figure 13

The results of the flattest model inversion:

(a) The model which corresponds to N=45 (N^0-N=55), χ^2_S standard deviation=0.01.

(b) the model which corresponds to N=10 (N^0-N=90), standard deviation=0.01.

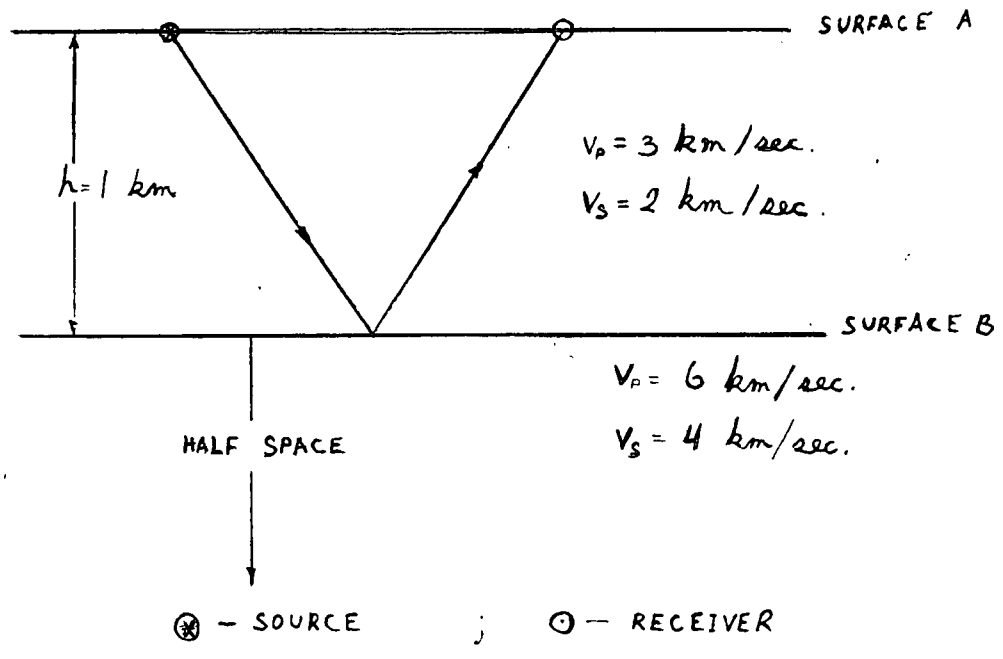

Figure 14

The model from which the synthetic seismogram of Figure 15(a) was generated.

achieve a complete recovery of the reflectivity sequence. The source wavelet and the recovered reflectivity sequence are shown in Figures 15(b) and (c), respectively. Examining the recovered reflectivity sequence we find that the spike of relative amplitude 0.2 which appears at about 14 time units is noise generated by the MED algorithm. Since we generally do not have this information, we include that spike in our input spike trace Y. The spikes which correspond to the rays specified above are well located but contain serious amplitude discrepancies. The MED output Y^0 was truncated from both ends as indicated by the

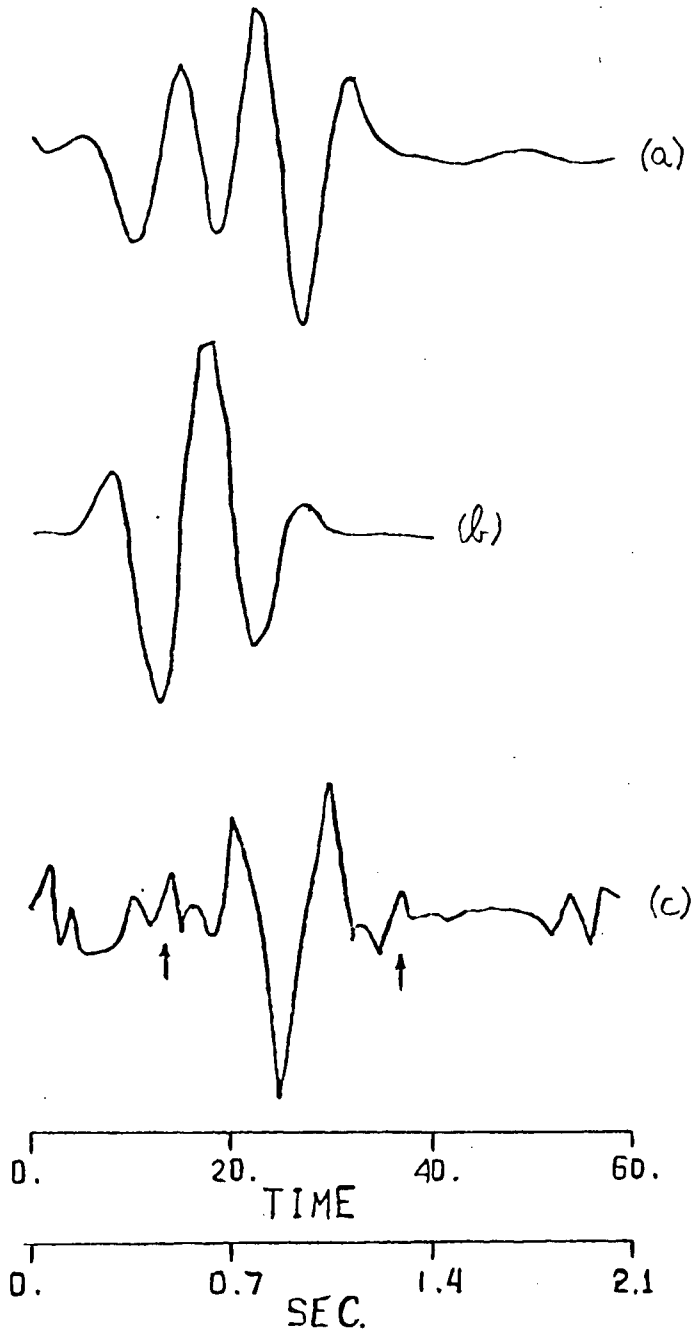

Figure 15

(a) The input trace X which is the synthetic seismogram of the model in Figure 14. (b) The source wavelet. (c) The MED output, the trace Y, which is the result of the convolution of the MED filter with X. Arrows mark the section used in the inversion.

arrows in Figure 15(c). The resultant spike trace Y and the input trace X (Figure 15(a)) served as input to the linear inversion schemes.

A plot of the standard deviation versus N^0-N for the flattest model was calculated and is plotted in Figure 16(a). In this example the practical rank of the inner product matrix is 36, and $N^0=58$. Note the flat region corresponding to $22<N^0-N<46$. Since all those models which corresponds to $36>N>12$ reproduce the observations to within the same standard deviation, we will represent all those models by two models corresponding to the ends of the region. These are shown in Figure 17(a) and (b).

Plots of the maximum error and standard deviation (Figure 16(b) and (c)) for the generalized linear inverse procedure also have been prepared. In Figure 16(b), we can distinguish two regions where the maximum error is approximately constant: $Q^0-Q<12$ and $12<Q^0-Q<26$. In Figure 16(c) the distinct regions where the standard deviation changes comparatively slowly are: $Q^0-Q<19$ and $19<Q^0-Q<26$.

Since the regions determined from Figures 16(b) and (c) do not coincide, we will have to represent the generalized linear inverse models by three models corresponding to the different regions given above. These representative models are shown in Figure 17(c) to (f).

The models shown in Figures 17(a) and (c) correspond to the flattest model with N=34, and the generalized linear inverse model with Q=33, respectively. These are models which are composed of nearly all positive values and hence are unphysical

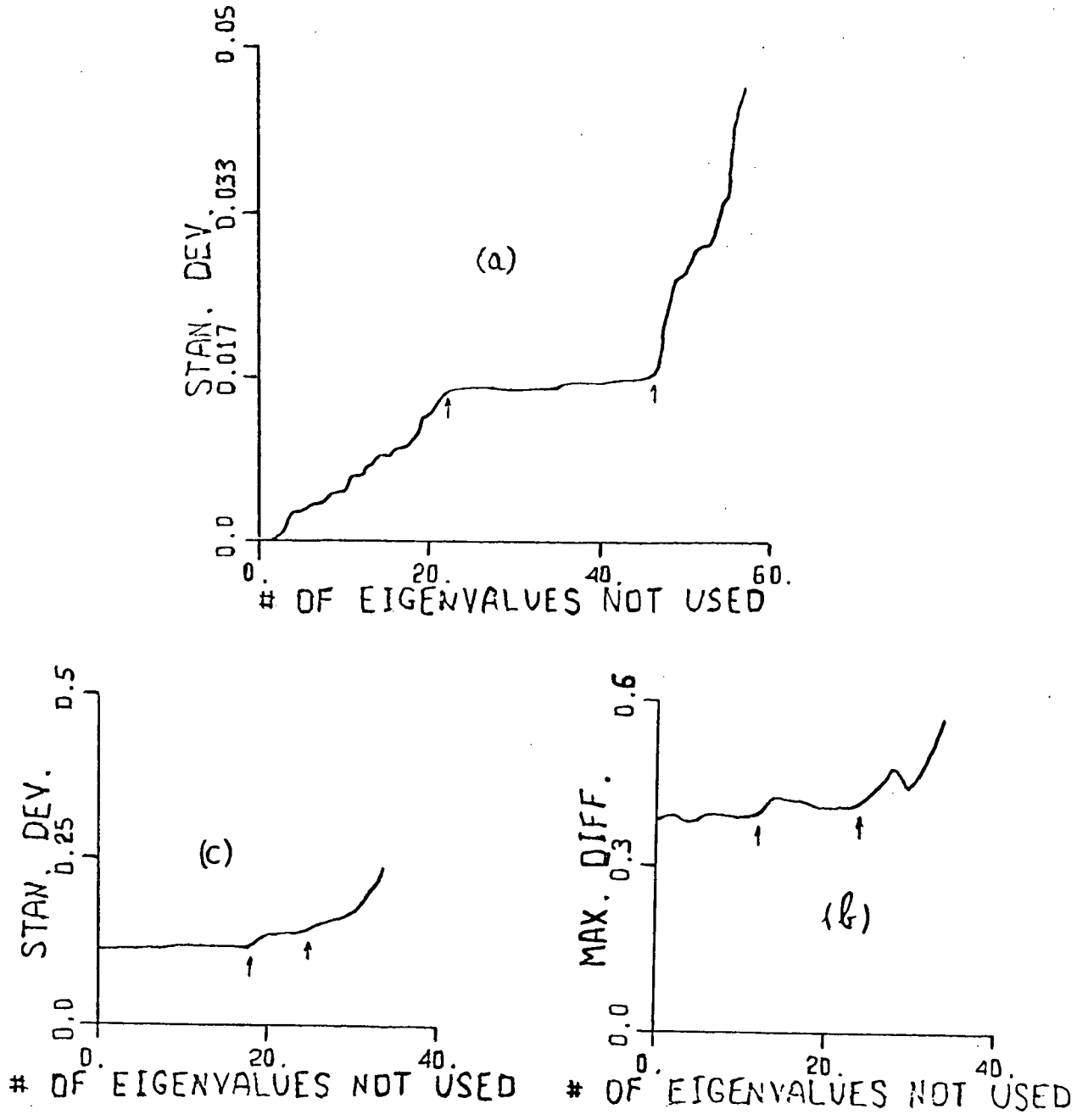

Figure 16

(a) A plot of N^0-N versus standard deviation for the flattest model.

(b) A plot of $Q^0 - Q$ versus $\text{Max}\{|\Delta x_i|\}$, for the general linear inverse.

(c) A plot of Q^0-Q versus standard deviation , for the general linear inverse.

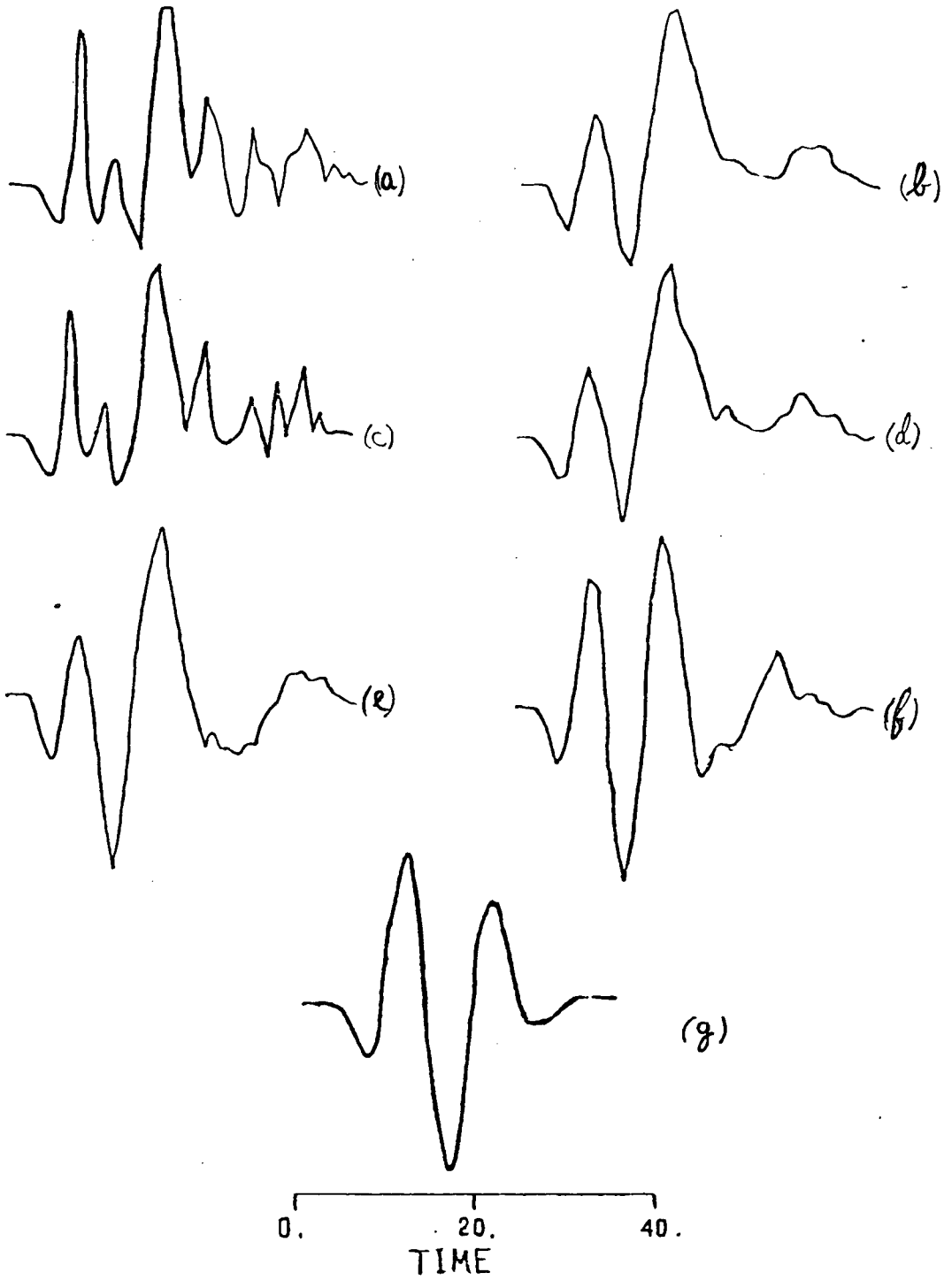

Figure 17

(a) The flattest model with N=34. (b) The flattest model with N=16. (c) The general linear inverse model with Q=33. (d) The general linear inverse model with Q=21. (e) The general linear inverse model with Q=15. (f) The general linear inverse model with Q=7. (g) The input wavelet reversed in polarity.

because we expect the wavelet to include positive and negative values. That is, we expect tensional stresses to fcllow compressional stresses or positive displacements to be followed by negative ones. Therefore these models are abandoned on physical grounds.

The remaining model wavelets shown in Figure 17 describe the source wavelet of Figure 15(b) with varying degrees of accuracy. All of these models provide a consistent description of the general features of the source wavelet in the region 7 to 21 time units. However the wavelet of (e) which is the general linear inverse model with Q=15 and the wavelet of (f) corresponds to the drop in $\text{Max}\{|\Delta X_i|\}$ in Figure 16(b) (Q=7), represent the true wavelet more closely and either could be chosen as an appropriate representation.

CONCLUSION

In this chapter we have shown that the linear inversion schemes are capable of extracting a great deal of information from a wide variety of input data. We concentrated particularly on seemingly unreliable data since that is where we could show the full power of the linear inverse techniques.

The smallest model inversion has proved inferior for this particular problem, probably because we represented the spike sequence Y as a series of box cars.

The flattest model approach performed slightly better on example B, while the general linear inverse scheme gave somewhat

better results in example C. Both techniques determined the main features of the input wavelet (in the case of example C, the region between time units 10 to 20 in the solution models). Since two integrations are involved in the Backus-Gilbert flattest model calculation, we expect that the error will be smoothed out. This will happen only if the spike input Y is a "high frequency" trace ; in other words only if the wavelet length is large compared to the dominant pericd in the spike trace. It is probable that the flattest model didn't perform as well in example C, because of the predominant lcw frequency of the spike trace Y of that example. Past experience with MED output shows that, in general, we can expect the dominant period in the MED output to be small compared to the wavelet length. Hence we can expect substantial smoothing of the error in the flattest model scheme.

Since the generalized linear inverse is a parametric approach it does not require continuous representation for the MED output. Also it does not involve integrations and hence seems to be computationaly simpler. However, the method requires decomposition of an nXm matrix which needs more computer time then the square matrix decomposition required by the Backus-Gilbert approach. For Q equal to the practical rank of A and N equal to the practical rank of Γ , the models generated by the generalized linear inverse and flattest mcdel are almost identical.

We demonstrated the importance of the plots of maximum error and standard deviation versus the number of eigenvalues not used in the solution , and showed how such plots can be used

to reduce the practical number of models. At this time, it is not possible to suggest an analytical way to enable the user to choose the best model out of the given group's representative set. The user will have to try each group's representative model as a possible estimated wavelet.

However, one might get some indication on the quality of the estimated wavelet, by formulating a new linear inverse problem of the form:

$$\bar{X}=\bar{W}^{i}*\bar{S}^{i}$$

where * denotes convolution and

X is the observation vector,

$\bar{W}^{i}$ is the i^{th} estimated wavelet vector, and

$\bar{S}^{i}$ is the i^{th} recovered spike sequence.

Then one solves for the spike sequence $\bar{S}^{i}$. Having the set of spike sequences $\bar{S}^{i}$ one calculates the associated set of varimaxes V . The "best" estimated wavelet is the one which is associated with the highest varimax trace $\bar{S}^{i}$.

CHAPTER 4

Debubbling as a Generalized Linear Inverse Problem

INTRODUCTION

The bubble pulse problem is common to many marine energy sources and has been discussed in detail by Kramer et al (1968). The problem is caused by successive oscillations of the gas bubble generated by the energy source. Each cycle of the oscillating bubble corresponds to a signal propagating outward. The source wavelet as recorded on a seismic trace is then a train of the wavelets generated by the individual cycles. The number of pulses and their periods are primarily a function of detonation depth and energy released during creation of the bubble. The length of the compound wavelet depends on the number of expand-collapse cycles of substantial energy generated by the bubble, until it has completely collapsed inward or vented remaining energy to the atmosphere. Duration of the compound wavelet often exceeds 0.5 sec. This excesive length creates severe interference problems and causes masking of events, especially on those parts of seismograms following large amplitude reflections.

The aim of debubbling schemes is to eliminate the bubble pulse effects, and to compress the compound wavelet signature to one that is simple and of short duration. Mateker (1971) suggested a debubbling scheme which shapes the recorded source

wavelet into a pulse at the time of the initial pulse. This process can be carried out through the use of the Weiner shaping filters. Recently, Wood et al (1978) suggested two closely related methods. The first can be described by the fcllowing stages :

1. Crosscorrelate the data and the known source signature. The resultant trace has a better signal tc noise ratio, and its wavelet is the autocorrelation of the source signature. The new wavelet is a zero phase one.

2. Using Weiner filters (Treitel and Robinson, 1966), shape the autocorrelated source wavelet into a short duration desired signal. When shaping the autocorrelated wavelet use the fact that it is a zero phase wavelet, one of the advantages of the crosscorrelation of step 1.

3. Apply the shaping filter of step 2 to the crosscorrelated data.

The second is similar and can be described briefly as follows:

1. Crosscorrelation of the known source signature with the data (as in step 1 above).

2. Compute the zero delay Weiner inverse filter of the wavelet and apply it to the data.

3. Crosscorrelate the zero delay Weiner inverse filter of step 2 with the data.

As seen from the above discussion, currently used debubbling methods employ Weiner shaping filters in their algorithms. These depend critically on the chcice of the length of the filter (an unknown parameter), and cannot overcome problems which arise due to errors in the recorded wavelet.

In this work, a new and different approach to the debubbling problem is presented. It makes use of the theoretical concepts embodied in generalized linear inversion (Wiggins et al 1976; also see Chapter 3). This technique is applied first to an estimation of the wavelet and secondly to the debubbling of the seismic trace using the estimated wavelet.

Debubbling as a generalized linear inverse problem is described by the following steps, and shown schematically in the flow diagram of Figure 1.

1. Apply minimum entropy deconvolution (Wiggins 1977; also see Chapter 2) to the observed data to get the deconvolved spike trace.

2. Use the deconvolved spike trace and the data as an input to the generalized linear inverse procedure to compute the estimated bubble pulse wavelet.

3. Use the information acquired in steps 1 and 2 to construct the compound source signature (i.e. the initial pulse plus appropriate bubble oscillations).

4. Use the compound source signature and the observed data as input to the generalized linear inverse scheme to determine the estimated earth impulse response.

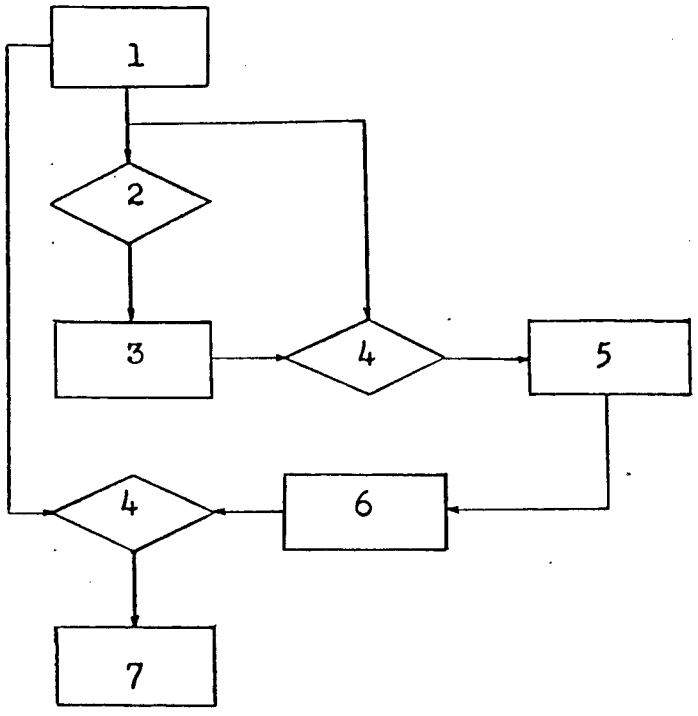

Figure 1

1. Data.
2. MED.
3. Deconvolved spike trace.
4. Generalized linear inverse.
5. Estimated wavelet.
6. Construction of the compound signature.
7. Debubbled trace

Flow diagram of the proposed debubbling procedure.

SOURCE SIGNATURE ESTIMATION AND DEBUBBLING

The assumption that a seismogram can be modelled as the convolution of the earth's impulse response with a source wavelet provides the basis for this work. Mathematically the statement is

$$X=S*W \qquad (1)$$

where X is the observed seismogram,

S is the earth impulse response and

W is the source wavelet.

In summation notation equation (1) takes the form

$$X_j = \sum_{k=1}^{m} W_k \cdot S_{j-k+1} \qquad (2)$$

j=1.....n, n is the length of the observed data;

k=1.....m, m is the length of the wavelet; and

the relation n=l+m-1 must hold, where l is the length of the earth's impulse response.

Having the observed data (the seismogram) and either the source signature or an estimate of the earth's response, one can solve for the unknown time series. For the sake of the discussion let us assume that we have the seismogram X and an estimate of the source signature W. Writing equation (2) in its matrix form we get :

$$\bar{X} = A * \bar{S} \qquad (3)$$

where

$$A(i,j) = W(i-j+1) \qquad j=1....l \;\; ; \;\; i=1....n \qquad (4)$$

with

$$W(i-j+1) = 0 \quad \text{for} \quad i-j+1<0 \text{ and } i-j+1>m$$

Equation (3) represents an overdetermined system in which n>l, i. e. the number of equations is larger then the number of unknowns. We solve this system of equations by minimizing the error vector $\bar{\Delta X} = \bar{X}^{OBS} - \bar{X}^{CAL}$ in a least squares sense. For a more detailed discussion the reader is referred to Chapter 3.

The least squares solution of (3) is given by :

$$\bar{S}^{*} = V_{q} \Lambda_{q}^{-1} U_{q}^{T} \cdot \bar{X} \qquad (5)$$

or in summation notation

$$S^{*} = \sum_{k=1}^{q} \bar{V}_{k} (\lambda_{k}^{-1} \bar{U}_{k}^{T} \cdot \bar{X}) \qquad (6)$$

where

U^{T} is the transpose of U which consists of q eigenvectors of length n associated with the columns of A; these vectors are commonly referred to as the data eigenvectors.

V consists of q eigenvectors of length 1 associated with the row vectors of A; these are commonly referred to as the parameter eigenvectors.

Λ^{-1} is the inverse of Λ which consists of the q eigenvalues of A in descending order. $\Lambda = \text{diag}\{\lambda_1, \lambda_2 \ldots \lambda_q\}$ where q is the rank of A.

Equation (6) states that the desired earth response is a weighted summation of the parameter eigenvectors. It is advantageous to use equation (6) as our solution, particularily when one is dealing with noisy data or when the estimated source signature is contaminated by noise. In both cases one could choose to reject the smaller and less reliable eigenvalues before proceeding with the calculations (see Chapter 3). This is easily done by letting Q in equation (6) assume smaller and smaller values. It is clear that the euclidian length of the error vector $\bar{\Delta X}$ grows as we reject more and more of the smaller eigenvalues, but at the same time we eliminate the less

reliable components of the solution. A useful tool in the analysis of the different solutions (corresponding to different Q values) is the plot of the standard deviation ($|\Delta X|^2$) versus the number of eigenvalues rejected (see Chapter 3).

In the alternative case where one has the seismogram X and the estimated earth response S, the only change in the above equations occurs in the definition of A. Then A is given by :

$$A(i,j)=S(i-j+1) \qquad j=1....m \;\; ; \;\; i=1....n \qquad (7)$$

where

$$S(i-j+1)=0 \quad \text{for} \quad i-j+1<0 \text{ and } i-j+1>1 \; .$$

Equations (5) and (6) still hold with W replacing S.

The flow diagram of Figure 1 outlines the procedure which is followed to obtain a debubbled seismic trace. Let us examine the various steps.

Having the field trace, we aim first at an intermediate target - estimation of the wavelet. To estimate the wavelet we require a rough estimate of the earth's response. To find that estimate we apply MED to the data. This leads to step 1 in the computation procedure.

1. Apply minimum entropy deconvolution (Wiggins 1977 ; also see Chapter 2) to the field data. The MED output serves as a first approximation to the earth's impulse response.

A troublesome point in step 1 concerns the choice of the length of the MED filter. Long MED filters tend to compress much of the energy in a trace into one large spike, this

overspiking being an undesirable feature. Short MED filters will recognize only the basic bubble pulse signature as the source signature and hence each event will be represented by the spikes associated with that signature. Figure 2 illustrates the latter statement. All the short MED filter has done is to "spike up" the appearance of the bubble wavetrain. However, this situation is preferred to one in which information might be lost. Then in general a short MED filter is used.

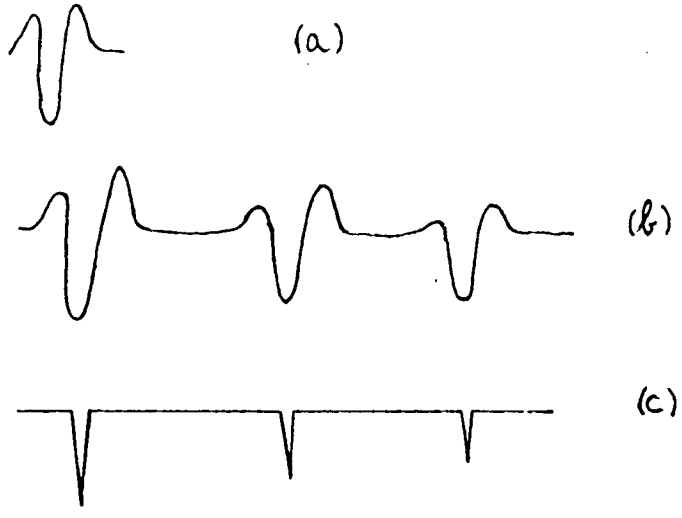

Figure 2

(a) Primary bubble pulse signature. (b) Compound wavelet signature (bubble pulse oscillations). (c) The output of the convolution of a short MED filter with the compound wavelet.

Having a rough estimate of the earth's response we are now in a position to continue to step 2 - estimating the wavelet.

2. Using the observed data X and the short filter MED output S as an input to the generalized linear inverse method, we estimate the basic bubble pulse signature W'.

Note that in stage 2 we prefer to use a short MED filter since a long filter will overspike the data and will cause a significant loss of information. The use of a short MED filter results in an estimated wavelet signature corresponding to one individual basic bubble waveform. As described in step 3, this wavelet serves as the basic form from which the bubble pulse wave train is constructed.

3. Examine the MED output and the observed data and identify those events which have been generated by the bubble pulse. Bubble pulse events on a T-X diagram do not show differential moveout as the distance changes. One then looks for parallel hyperbolas corresponding to the primary and the bubble pulses as sketched in Figure 3. Reflection events will show differential moveout relative to the bubble oscillations. On a T-X diagram they will appear as converging hyperbolas as shown in Figure 4.

Using the MED output and the data one can measure the bubble periods ΔT_i and estimate the relative amplitudes. Accurate estimation of the bubble pulse periods ΔT_i is important; however, relative amplitude estimates are not as important and will not influence critically the results. From the bubble oscillation periods, the corresponding relative amplitudes, and the basic pulse wavelet, the repetitive bubble pulse wave train can be constructed. This leads to step 4.

4. Using the observed data X and the compound wavelet signature W as an input to the generalized linear inverse scheme, we obtain an estimate of the earth's impulse response. This response does not include any of the secondary bubble

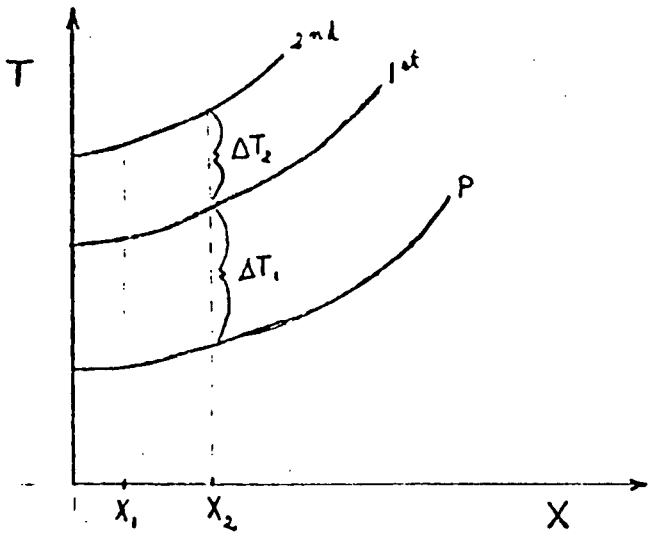

$$\Delta T_1\Big|_{X_1} = \Delta T_1\Big|_{X_2}$$

$$\Delta T_2\Big|_{X_1} = \Delta T_2\Big|_{X_2}$$

Figure 3 - Bubble pulse events do not show differential moveout - the branches corresponding to such events will be parallel.

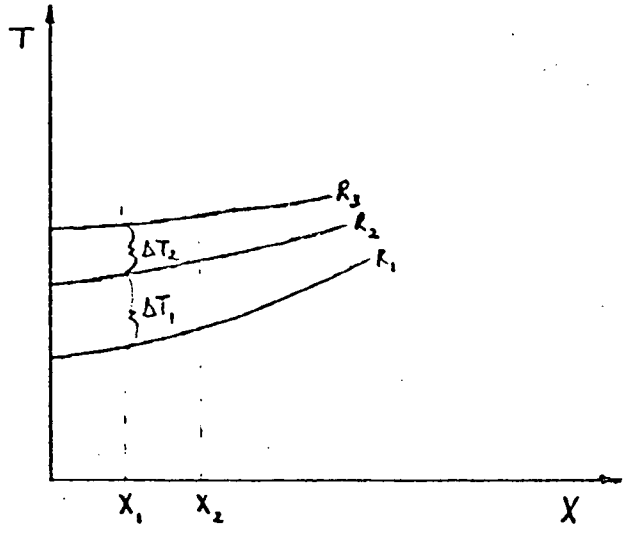

$$\Delta T_1\Big|_{X_1} \neq \Delta T_1\Big|_{X_2}$$

$$\Delta T_2\Big|_{X_1} \neq \Delta T_2\Big|_{X_2}$$

Figure 4 - Reflection events on a T-X diagram show differential moveout.

oscillations; the original complex bubble pulse signature collapses to a single 'spike' in the earth response. Note that step 4 is simply the reverse of step 2.

EXAMPLES

A. Synthetic Seismogram

The first example that will be shown demonstrates only step 4. Steps 1 and 2 were discussed in detail in Chapters 2 and 3, and step 3 will be demonstrated in the next example.

Synthetic seismograms for the simple model shown in Figure 5 have been generated using generalized ray theory (Wiggins and Helmberger 1974). This model is a simplification of a situation one may encounter when exploring the depth of the sediments in a deep water region. Model characteristics are summarized in Table I.

TABLE I

Model characterisics for calculation of synthetic seismograms.

	Thickness (km)	Depth (km)	P-velocity (km/sec)	Density (gm/cm^3)
Water	1.5	1.5	1.5	1.0
Sediment	0.75	2.25	3.0	2.0
Basalt layer	half space	half space	6.0	3.0

In this example, the primary P reflections with vertical travel times of 2 sec for the sea bottom reflection and 2.5 sec for the reflection from the base of the sediments will be considered. The compound wavelet which has been used (Figure 6) was constructed to simulate an energy source which sends out a primary signal followed by two bubble pulses. Relative amplitudes and the corresponding bubble periods are shown in Figure 6. Total length of the compound wavelet is 0.6 sec. These wavelet characteristics were chosen because of the similarity with the expected characteristics of the field example to be described next.

Eight synthetic traces were generated corresponding to offsets between 0.2 km and 1.6 km with receiver separation of 0.2 km. The traces were normalized such that the largest amplitude in each trace was unity (Figure 7). Relative amplitudes for reflections from the base of the sediments range from 0.22 for the near vertical reflections to 0.1 for the widest angle reflections. Numerical noise level in the synthetic seismograms increases with the offset as a result of longer calculation intervals. Note that the type of behavior shown in Figures 3 and 4 is clearly observed in this synthetic example. In particular, the reflection from the base of the sediments is hidden by the bubble pulse events on traces 1 to 4 while it can be observed from traces 5 to 8.

The synthetic seismograms of Figure 7 and the bubble oscillation wavelet of Figure 6 formed the input to the generalized linear inverse scheme as discussed in step 4. The debubbled seismograms determined from application of the inverse

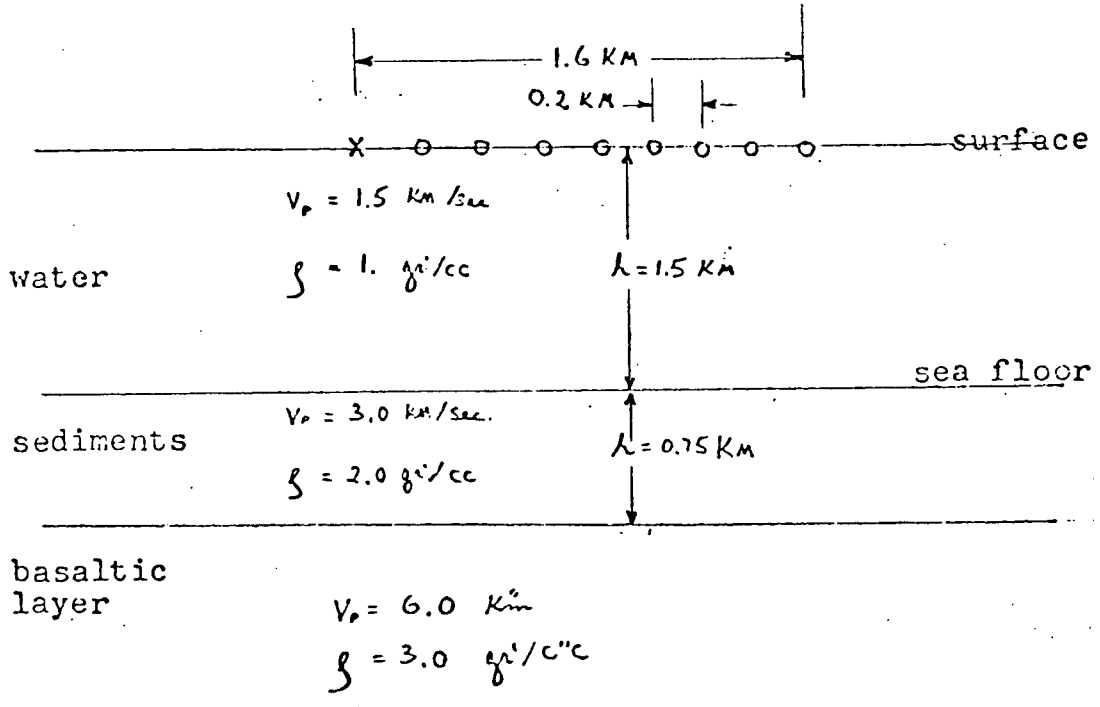

Figure 5 - The layer model used in the construction of the synthetic seismogram.

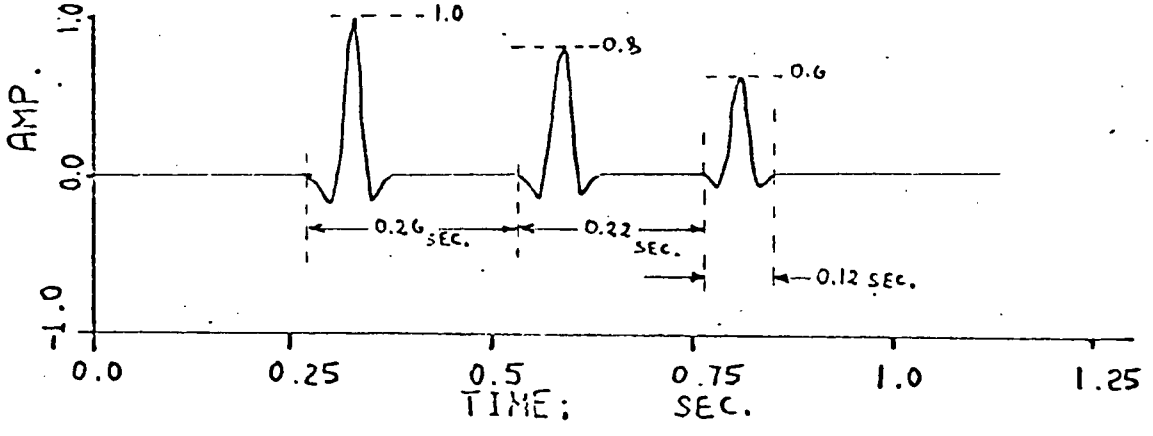

Figure 6 - Signature of the compound source wavelet used to generate the synthetic seismogram.

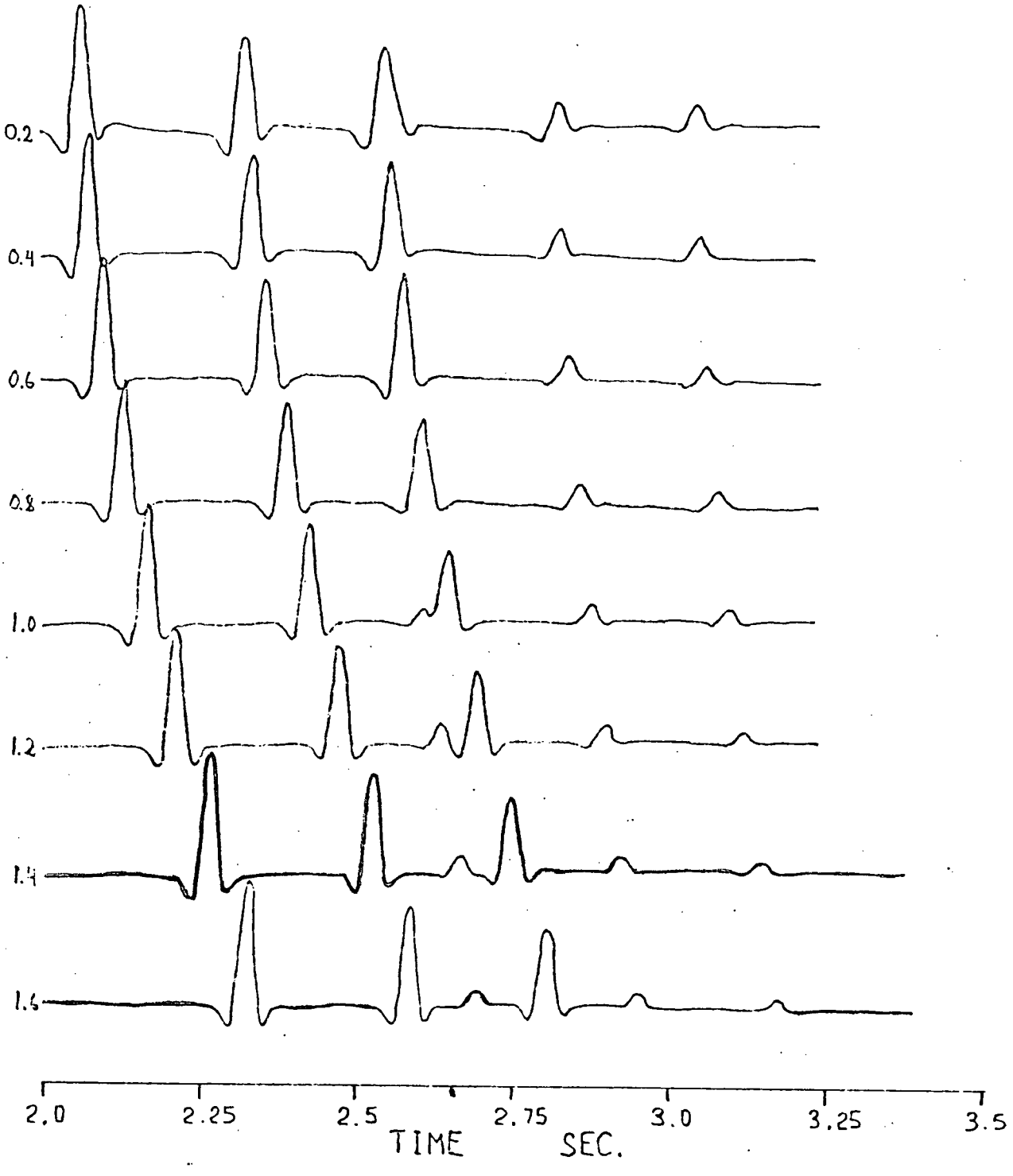

Figure 7 - Synthetic seismogram (generalized ray theory) based on the model of Figure 5. The source wavelet is shown in Figure 6.

procedure to each trace is shown in Figure 8. Two major effects are noted. First, the extended bubble pulse oscillation wave train has been reduced to just one pulse, and further this pulse has been compressed to have a greater 'spike-like' character. Also, as the numerical noise level increases, the solution becomes more oscillatory as evidenced by traces 7 and 8. On these traces, the reflection from the base of the sediments shows only marginally above the background noise level.

Considering that the ratio of the smaller amplitude reflection to the larger one in traces 7 and 8 is about one to ten and that these traces include noise with a maximum amplitude of about 50% of the smaller reflection amplitude, the results of Figure 8 form a good output.

B. FIELD EXAMPLE

Clowes et al (1978) and Thorleifson (1978) have described a marine deep seismic sounding program carried out in Winona Basin, a deep water (2 km) sedimentary basin located west of northern Vancouver Island, British Columbia. Signals from six individual hydrophones separated by 90m and suspended at 45m depth from a 600m cable trailed behind the receiving ship were recorded digitally while the shooting ship detonated explosive charges ranging in size from 2.2 kg to 200 kg at distances from less then 1 to 95 km. Clowes (1977) has described the system in

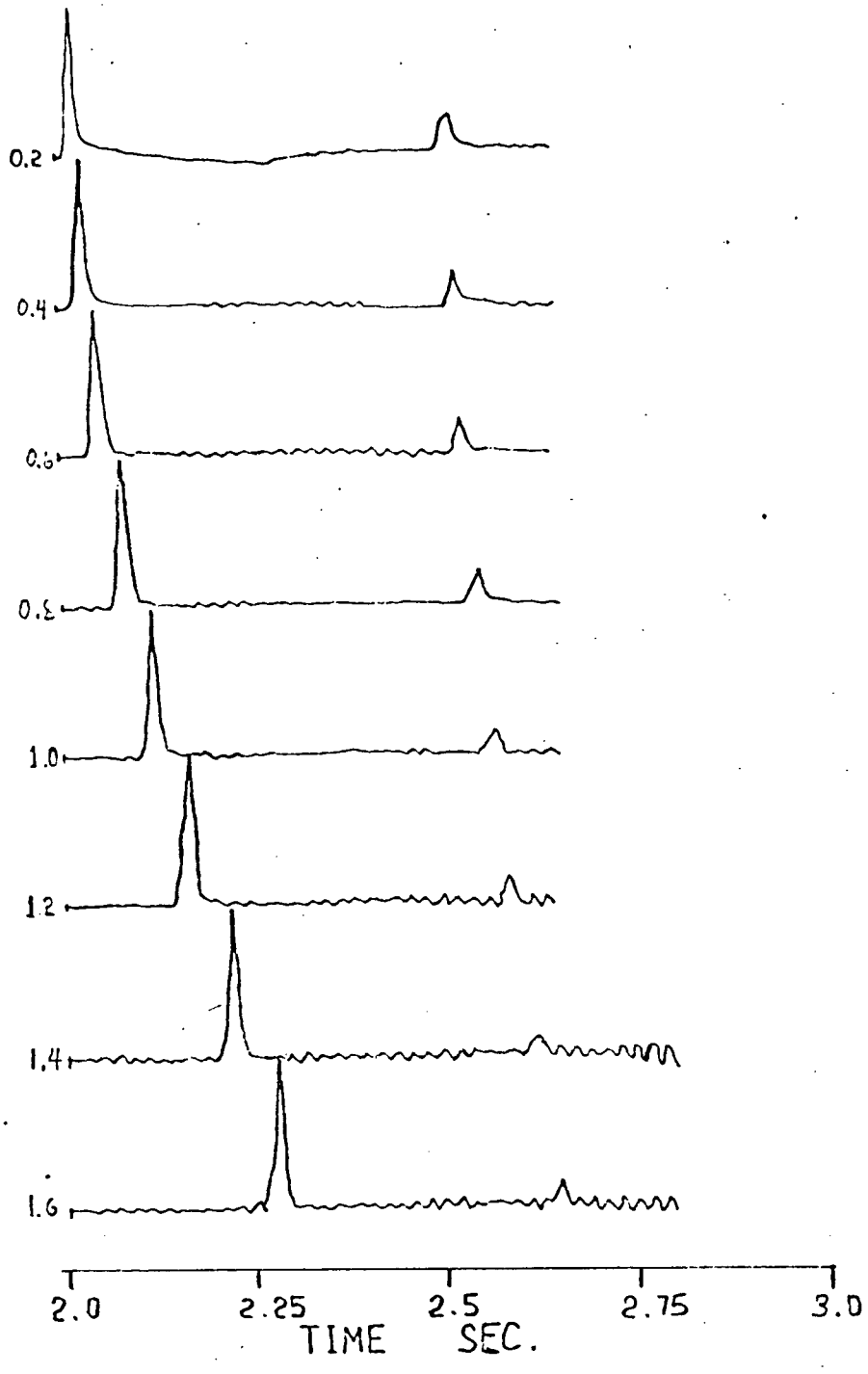

Figure 8 - The estimated earth's response calculated by the generalized linear inverse scheme.

detail.

Seismograms from 2.2 kg shots were detonated at 7m and recorded at distances up to about 6 km to form sub-critical incidence reflection profiles. Thorleifson (1978) has described the interpretation of some of these. Six traces from one shot have been extracted from one profile and are shown in Figure 9. For the purposes of this study, these traces have been normalized such that the maximum amplitude in each trace has a relative amplitude of 1.0. The data are bandpass filtered from 5 to 30 hz.

The most prominent arrivals are the water bottom reflection with its associated bubble oscillations as indicated on the figure by W, W^1 and W^2. By carefully looking at differential moveout between different phases for many correlatable cycles, Thorleifson (1978) was able to identify some primary reflections from within the sediments of Winona Basin. His identification of these events is shown by the letters A, B and C on Figure 9. We note that the bubble pulse wave train shows the characteristics described in Figure 3, while the primary reflections show those depicted in Figure 4.

From Figure 9, it is clear that the source wavelet with bubble oscillations can be constructed from the primary pulse followed by two bubble pulses. The first step in our debubbling-pulse compression procedure is to estimate the basic bubble pulse signature in every trace. We do not expect only one basic bubble signature to hold for the different traces since each of these corresponds to different angles of incidence. The phase shift problem might be circumvented by use

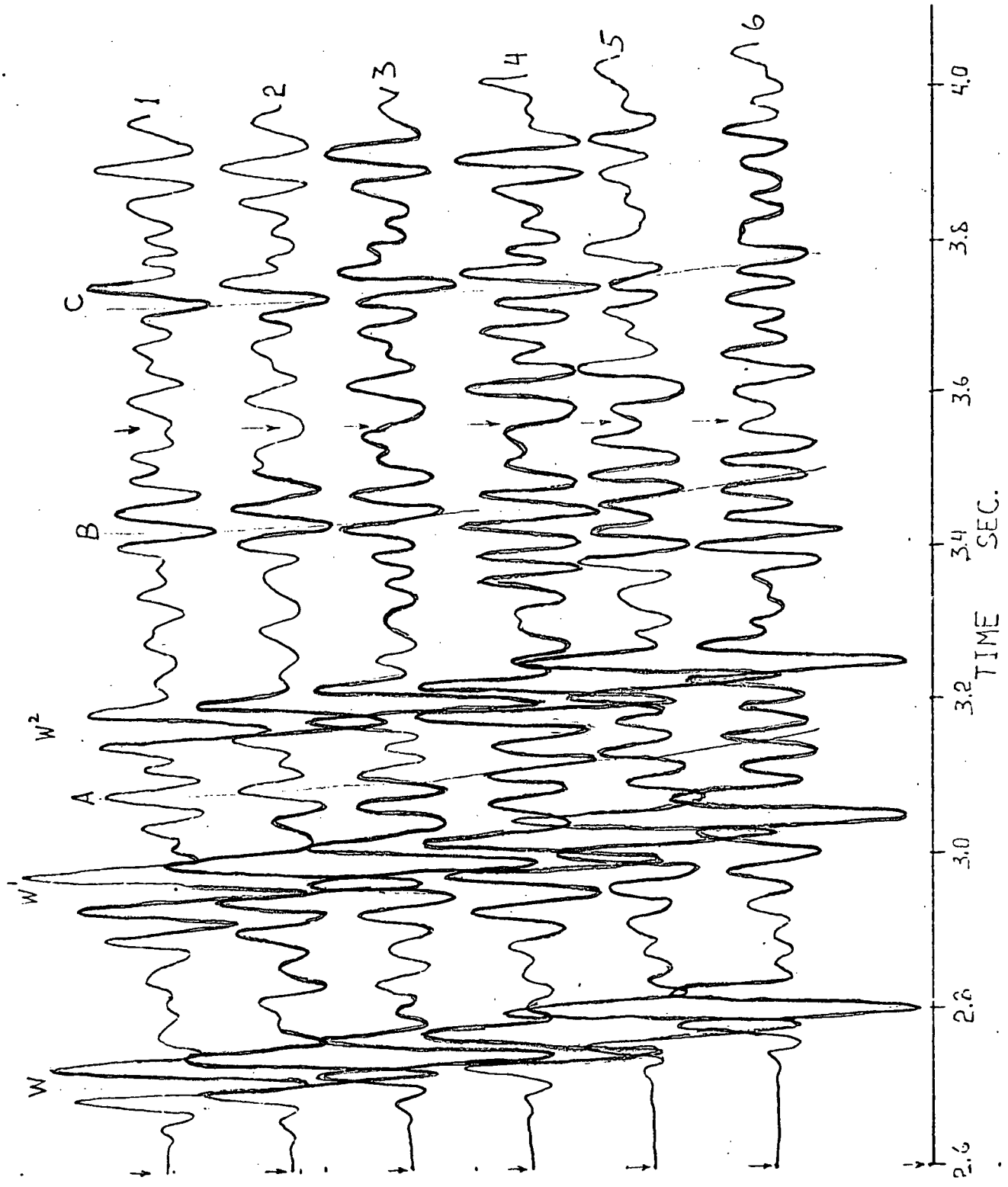

Figure 9 - Six traces from a reflection profile recorded off Vancouver Island. Traces are at distances from 1.0 to 1.5 km. Each trace is normalized to unit amplitude.

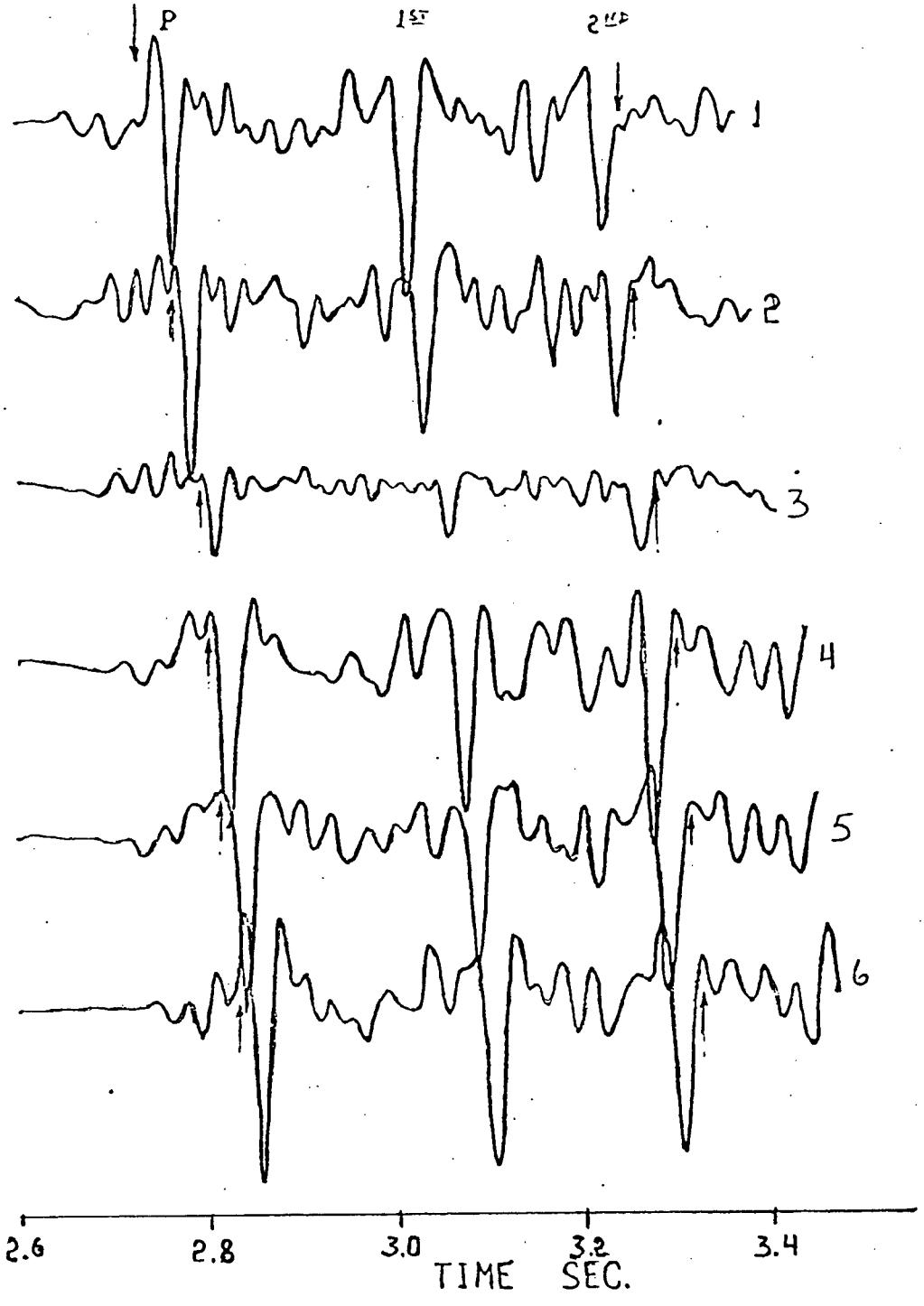

Figure 10 - Output traces from the single channel minimum entropy deconvolution procedure applied to the seismogram of Figure 9.

of the envelopes of the analytic signal (Clayton et al 1976). However, in this work we prefer to calculate the actual wavelets from which the individual traces are generated.

Applying the "short" length MED filter to the data shown in Figure 9, one gets the spiked outputs of Figure 10 which serves as a first approximation to the earth's response. Because phase shifts are expected, different MED filters were applied to different traces. The parts of the spiked traces marked by arrows in Figure 10 with the corresponding parts of the data traces marked by arrows in Figure 9 were used to estimate the basic bubble signatures of Figure 11 as discussed in step 2. Distinct differences are easily observed between the different bubble pulse signatures. Note in particular the wavelet associated with the fifth trace corrresponding to offset of 1.4 km.

The basic bubble pulse signatures shown in Figure 11, together with the periods and amplitude information acquired from the MED output and the original data, are used to construct the compound wavelets as discussed in step 3. The bubble periods were estimated to be 0.26 sec for the first bubble pulse, and 0.22 sec for the second with basic pulse signature length of 0.12 sec. The total compound signature length is 0.6 sec, and the relative amplitudes that were used are: 1.0 for the primary pulse, 1.0 to 0.8 for the first bubble pulse and about 0.7 for the second. As mentioned earlier, the relative amplitude does not carry as much weight as the estimated bubble period, and will not affect the solution as critically. The compound bubble pulse wavetrain for trace 1 is shown in Figure

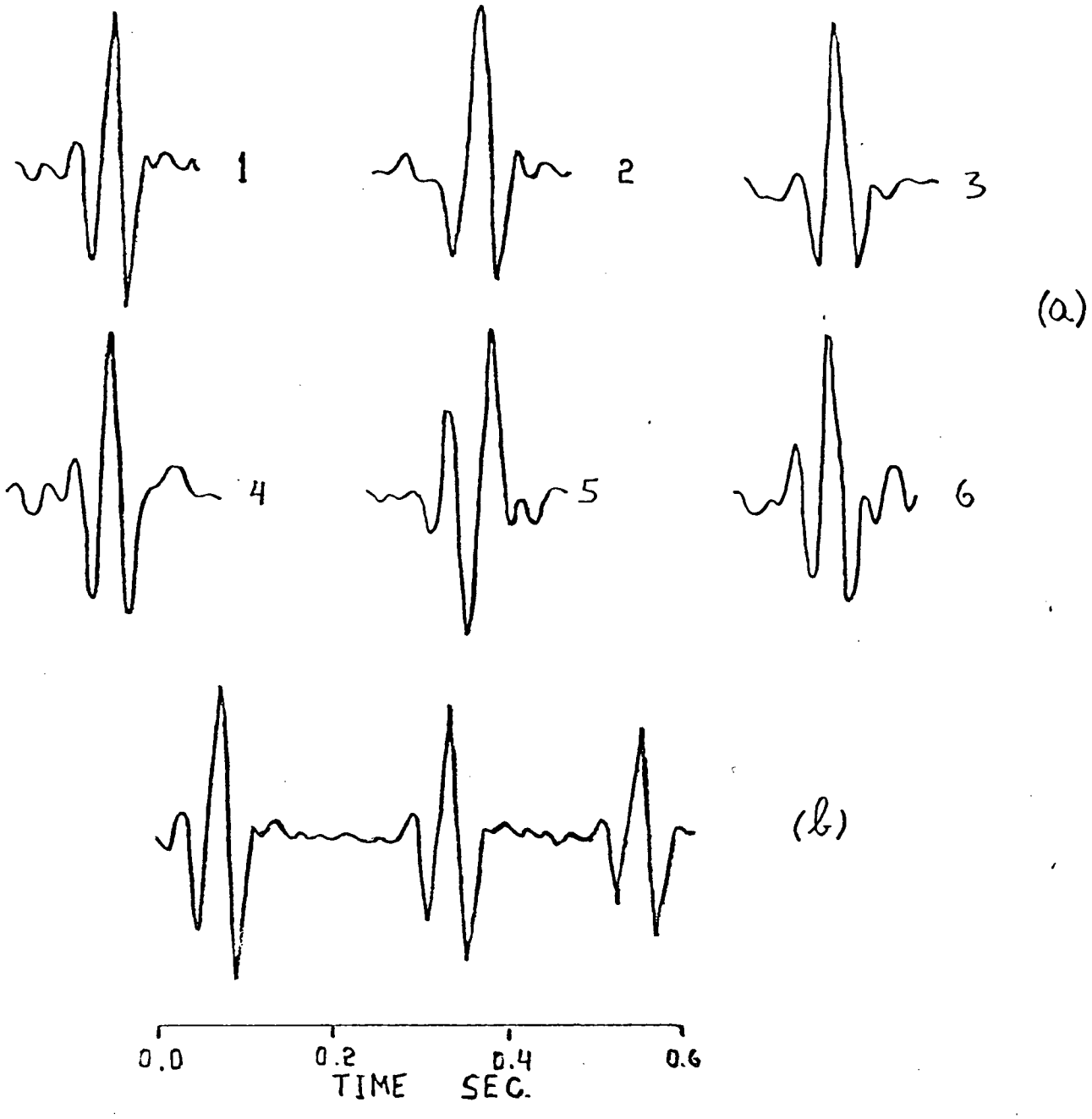

Figure 11 - (a) The basic bubble signatures associated with the different traces. Note in particular the phase shifted wavelet associated with the 5 trace. (b) Source wavelet for trace 1.

11(b). The remaining 5 compound wavelets have similar appearance after the construction which used the basic wavelets of Figure 11(a).

The compound wavelet signatures can be used together with the desired section of the recorded data, as described in step 4, in order to get the generalized linear inverse outputs i.e. the desired earth's response. The computed debubbled traces are shown in Figure 12.

It is easy to identify the five reflection events which dominate the section; these are marked in Figure 12 by W for the water bottom reflection, A^0, A, B, and C.

Figure 12 is a considerable improvement over the observed data shown in Figure 9. The ambiguity concerning the authenticity of some events has been removed and the output traces are considerably more spiky. In particular, one can now observe without any difficulty the events marked by A^0 and A which were completely or partially masked by the bubble pulses.

There are some differences in the level of performance of the scheme for the different traces. For example, consider event C. Traces 1,4,5,and 6 are of better quality then traces 2 and 3. However, for the most part, the events marked on Figure 12 are clear and continuous.

In the solution of this example, we did not reject any of the smaller eigenvalues, since at each stage of the operation we felt that the degree of reliability of our results was high. Convolution of the estimated wavelets with the estimated impulse responses gave calculated seismograms which differ from the field seismograms by a standard deviation of 0.15 to 0.20 when

Figure 12 - The estimated impulse response set (debubbled seismograms) calculated by the generalized linear inverse scheme. The polarity reversal of the output response in the fifth trace (offset is about 1.4 km) is due to the phase shifted wavelet. Reflection events are marked by W, A°, A, B and C.

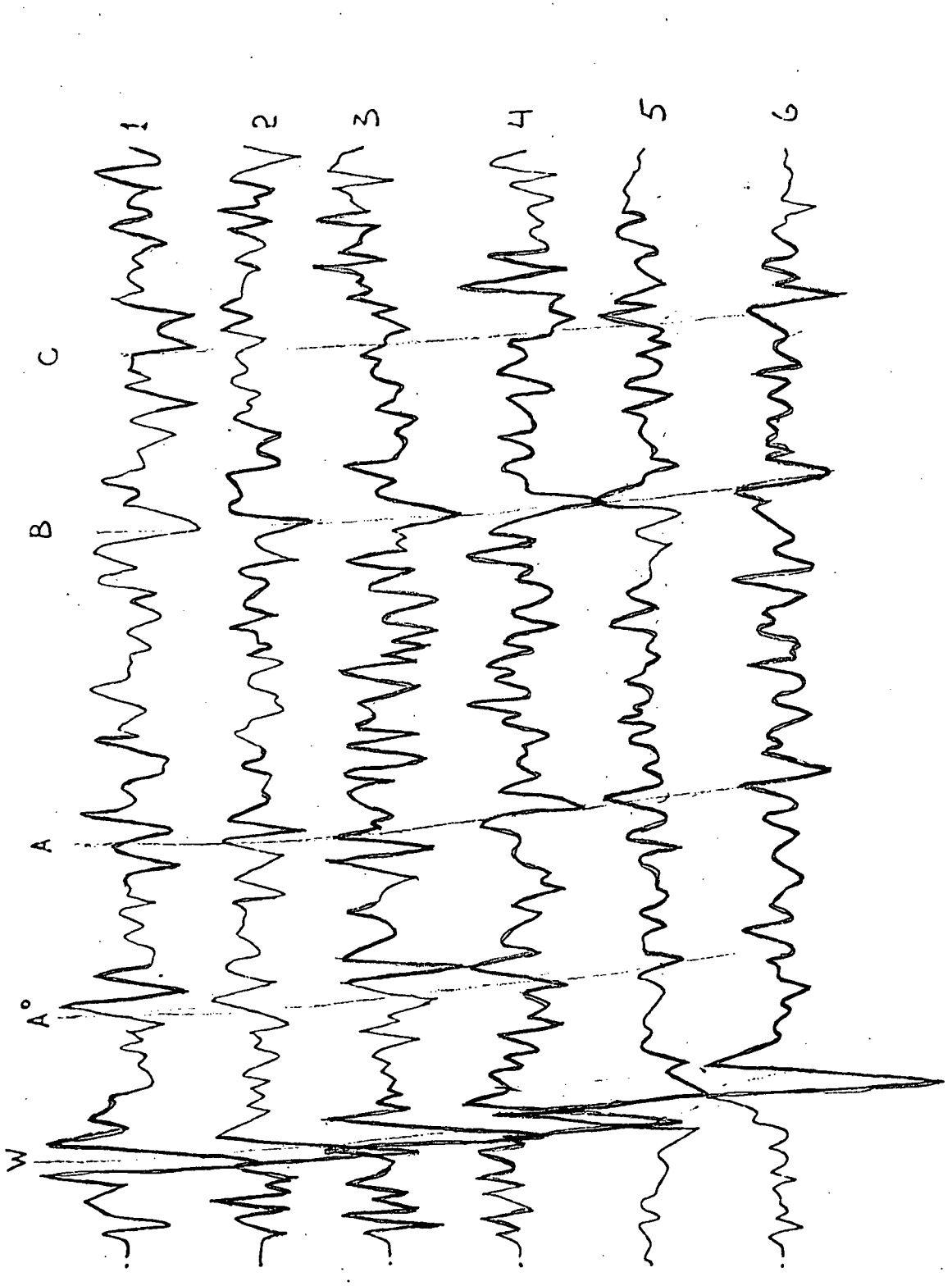
W
A°
A
B
C
1
2
3
4
5
6
2.6
2.8
3.0
3.2
3.4
3.6
3.8
4.0
TIME SEC.

normalized to a maximum amplitude of 1. We feel that such a standard deviation is acceptable and the debubbled traces are a better representation of the earth's response function, thereby enabling a better interpretation.

CONCLUSION

The generalized linear inverse scheme has been shown to be a useful tool for wavelet estimation and debubbling. We estimated the wavelet and used this estimate in our debubbling-signature compression procedure.

An attempt to deconvolve a trace given an error-contaminated wavelet by using Weiner filters or by dividing the trace's Fourier transform by that of the given wavelet will often result in erroneous outputs. We believe that the method described in this work increases the processor's ability to deal with noisy wavelets.

An important advantage of the generalized linear inverse scheme is that one does not (and can not) solve for the impulse response exactly. Rather, one gets the least squares solution. Since all of the equations in the deconvolution problem are weighted equally, the presence of errors in some of them will not necessarily result in erroneous solutions. Furthermore, using the properties discussed in Chapter 3, we are able to solve the deconvolution problem to within a prespecified standard deviation, provided that this standard deviation is

consistent with the given problem (one cannot get out of the data more then it has). The smallest standard deviation (S.D)min is achieved when all the eigenvalues are kept in the solution of equation (6). However, if (S.D)min is small compared to the estimated noise level, the mechanism of small eigenvalues rejection can be used. This mechanism allows us to solve problems with highly noisy observations, or highly noisy wavelets (see Chapter 3).

The proposed scheme treats debubbling and signature compression in one step and thus reduces the risk of accumulated error. (Although the singular value decomposition process is a time consuming one, it seems to be reasonably stable).

Since the wavelet signature within the same trace is time dependent, one may expect that an inverse filter, calculated for a certain time interval, may not perform acceptably in another time interval along the trace. The generalized linear inverse scheme is more flexible to errors in the wavelet and hence we expect that given a certain wavelet, the inversion scheme will be able to be used successfully over a longer time interval.

An important consideration in our scheme is the singular value decomposition process, which is a time consuming one and hence increases the cost of the inversion. In order to reduce the size of the problem, one has to increase the digitization interval, which in turn might reduce the solution's quality. However, in many cases the data are digitized at smaller intervals than what is really necessary. In such cases, increasing the digitization interval will result in considerable saving without any reduction in solution quality. In the field

example discribed above, we increased the digitization interval from 0.0032 sec to 0.0096 sec, included 2.0 sec of observed data with a 0.6 sec wavelet and obtained a response output of length 1.4 sec. Even with this data decimation, a matrix of the crder of 200 by 140 had to be inverted.

Our work and others (D.W. Oldenberg, personal comunication, 1979), suggests linear inverse methods may be quite successful in treating deconvolution problems in which noise is prevalent. Then, in cases where regular time series analysis techniques do not give acceptable results, the more computationally expensive inversion algorithms could be applied.

In this study we have approached the debubbling procedure as a generalized linear inverse problem. As discussed in Chapter 3, an alternative approach in which the problem can be formulated is the Backus-Gilbert technique. The application of this procedure might give even better results than those shown in this study.

REFERENCES

Clayton R.W, McClary B., and Wiggins R.A., 1976. Bull. Seism. Soc. Am., 66, 325-326.

Clowes R.M., 1977. A marine deep seismic sounding system, Can. J. Earth Sci., 14, 1276-1285.

Clowes R.M., Thorleifson A.J., and Lynch S., 1978. Interpretation of a marine deep seismic sounding survey in Winona Basin off the West Coast of Canada, Gecl. Surv. Can. Paper 78-1C, 29-34.

Harman H.H., 1960. Modern factor analysis, Univ. Of Chicago Press, Chicago.

Inman J.R., Ryu J., and Ward S.H., 1973. Resistivity inversion, Geophysics, 38, 1088-1108.

Jackson D.D., 1972. Interpretation cf inaccurate, insufficient and inconsistent data, Geophys. J. R. Astr. Soc., 28,

Kramer F.S., Peterson R.A., and Walters W.C., 1968. Seismic energy sources 1968 handbook, United Geophysical Corporation, 57p.

Lanczos C., 1961. Linear differential operators, D. Van Nostrand Co., London.

Lines L.R., and Ulrych T.J., 1977. The old and the new in seismic deconvolution and wavelet estimation, Geophys. Prosp., 25, 512-540.

Mateker E.J., 1971. Big benefits seen with maxipulse system use, Oil and Gas J., 69, 116-120.

Ooe M., and Ulrych T.J., 1979. Minimum entropy deconvolution with an exponential transformation, Geophys. Prosp. (in press).

Robinson E.A., 1967. Multichannel time series analysis with digital computer programs, Holden-Day, San Francisco.

Thorleifson A.J., 1978. A marine deep seismic sounding survey over Winona Basin, M. Ap. Sc. Thesis, Univ. Of British Columbia, 70p.

Treitel S., and Robinson E.A., 1966. The design of high resolution digital filters, IEE Trans., Geosci. Electrcnics GE-4, 25-38.

Ulrych T.J., Walker C.J., and Jurkevics A.J., 1978. A filter length criterion for minimum entropy deconvolution, J. Can. Soc. Expl. Geophys.,14, 21-28.

Wiggins R.A., Larner K.L., and Wisecup R.D., 1976. Residual statics analysis as a general linear inverse problem, Geophysics, 41, 922-933.

Wiggins R.A., 1977. Minimum entropy deconvolution, Proc. Int. Symp. computer aided seismic analysis and discrimination, Falmcuth, Mass., IEEE Computer Society, 7-14.

Wiggins R.A., Helmberger D.V., 1974. Synthetic seismograms by expansion in generalized rays, Geophys. J. R. Astr. Soc., 37, 73-90.